JKU

**JOHANNES KEPLER
UNIVERSITY LINZ**

TRANSPARENT ELECTROCHEMICAL TRANSISTORS DERIVED FROM POLYANILINE

Author
Kurt Aricanli

Submission
Institute for Physical Chemistry

Thesis Supervisor
Niyazi Serdar Sariciftci

Assistant Thesis Supervisor
Eric Daniel Glowacki

Month Year
March 2016
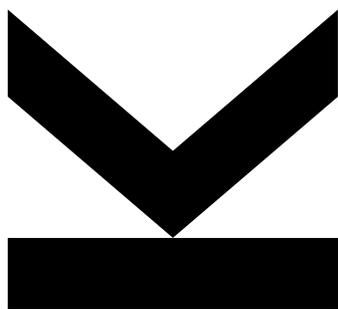
Master's Thesis

to confer the academic degree of

Diplom-Ingenieur

in the Master's Program

Wirtschaftsinginuerwesen Technische Chemie (WITECH)

Abstract

In this work, thin films of conducting polyaniline (PAni) are prepared by electrochemical percolation polymerization between two thin-film electrodes. The resulting films are several tens of nanometers thick, but can be up to tens of micrometers broad, giving an aspect ratio of 1000. The relationship between polymerization time and the percolation and film-growth and conductivity are evaluated in detail. Percolation between electrodes separated by 50 μm occurs at a surprisingly low value of ~ 9 s within the onset of polymerization, as proven by film conductivity measurements as well as scanning-electron microscopy. A relationship between the degree of film percolation and film transconductance is determined using electrochemical transistors. It was proven that the longer a film is allowed to percolate and the thicker the polymer layer is, the stronger the transistor modulation, *i.e.* on/off ratio. Transistor performance was also tested with respect to gel electrolyte thickness, electrolyte ionic conductivity, and level of hydration. These experiments show that bridge percolation occurs very rapidly during electropolymerization, in contrast to the prevailing knowledge in the literature, and further reveals the aspects of PAni-based electrochemical transistors.

Zusammenfassung

In dieser Arbeit, polyanilin (PAni) Dünnfilme wurden hergestellt mittels elektrochemisch perkolation Polymerisation zwischen zwei Dünnfilmelektroden. Die hierdurch entstandenen Filme haben eine Dicke um weniger als 150 nm, und sind mehr als 50 μm breit. Die Zusammenhang zwischen Elektropolymerisationszeit und Film-Wachstum wurde beobachtet. Filmen haben sich nach einer Elektropolymerisationszeit um 9 s auf glass gebildet. Die Abhängigkeit des Wirkleitwerts auf Elektropolymerizationszeit, Dicke des Gel-Elektrolyts, elektrolytische Ionenleitfähigkeit, und Hydrationsgrad wurde untersucht. Durch diese Experimenten wurde ein Polyaniline Dünnschicht hergestellt mittels einer Methode, die nicht in der Literatur zu finden ist. Zusätzlich, wurden die verschiedenen Facetten der PAni elektrochemischen Transistor untersucht.

Table of Contents

List of Figures

List of Tables

1. Objective

Characterize polyaniline-based solid-state electrochemical transistor devices, and optimize parameters of on/off ratio and transconductance as a function of polyaniline morphology and structure and device architectures. Electrochemical transistor devices are a major part of emerging bioelectronics technologies and revitalizing polyaniline for this purpose will be stimulating for the field.

2. Introduction

2.1 Conjugated polymers: a brief overview

In what has become an historical point in the industrial revolution, the dye mauvine, an oligomer of the molecule aniline, was discovered by William Henry Perkin in the 1850s. Its ability to stain silk was a major breakthrough in the dyestuffs industry, and its discovery opened the flood-gates for an entire field of color chemistry [1]. BASF – which was formerly called Badische Anilin und Soda Fabrik – also started as a dye industry, and its name is an everlasting tribute to the boom in aniline chemistry which took place following Perkin's discovery. Aniline-based molecules are still an important building block for many industrial colorants as well as other commercially-relevant chemical materials including pharmaceuticals and biomedical materials.

Prompted by Fritz London's notion of superconducting organic materials in 1937 [2], William A. Little justified the notion of superconductivity in unsaturated organic molecules on the whim that conjugated polymers could undergo excitonic excitations [3]. The discovery of *conductive* conjugated polymers was accredited to the combined efforts of Alan Heeger, Alan McDiarmid, and Hideki Shirakawa. Since this 1977 discovery, critical research has been done exploring the theory and application of conjugated polymers, as well as organic conjugated small molecules, fullerenes, and organometallic complexes. Among these materials, PAni remains one of the most thoroughly-studied. Overall, the field of organic electronics is extremely attractive due to ease of production, mechanical flexibility, and cost effectiveness in fabricating chemical

and biological sensors [4-6], artificial muscles [7], integrated circuits [8], memory [9], electrochromic devices [10], and organic photovoltaic cells [11-14], by which all semiconductors exist as thin films. Thin films of conjugated polymers can typically be produced via a medley of processes – chemical polymerization, electropolymerization, sublimation [15], epitaxy [16], spin-coating, and doctor blading [17] – and, there are many different conjugated polymer derivatives, all which give rise to a plethora of characteristics.

2.2 Applications of conjugated polymers in the realm of electronics

With the emergence of this technology, IBM in 1979 reported a *p*-type conductivity of polypyrrole (PPy) thin-films at room temperature of 100 S cm⁻ – more conductive than metallic germanium and silicon by three and six orders of magnitude, respectively. These films were formed via electrolytic oxidation of pyrrole and stayed conductive at temperatures of up to 250° C [18]. While PPy has been the most studied conjugated polymer in the realm of biosensors [7], various polythiophene (PT) derivatives including those such as poly(3,4-ethylenedioxythiophene): polystyrenesulfonic acid (PEDOT:PSS) [19], poly(3,4-(bis[2,2-methyloctadecoxy]-propylenedioxythiophene) (PProDOT(C_{18})$_2$) [10], and poly(3-hexylthiophene) (P3HT) [20], are all also very heavily utilized as semiconductors in sensing research as well as in other applications. PEDOT:PSS's printed water-soluble films have been demonstrated to function as a capacitor electrode material [21], transparent electrode material for light-emitting diodes (LEDs) [22], as a semiconductor in lactate and glucose sensors [23], and as electrochromic display active layer materials with on-off switching on the quarter-second scale [24]. Water-processible (PProDOT(C_{18})$_2$) films have been developed which form stable electrochromic window-type devices [10]. PAni is mainly used as a finish for corrosion-prevention on printed circuit boards (PCBs) due to its chemical nobility and ability to electrically shield the electrical components from static electricity. It is also used in ammonia sensors with sensing thresholds as low as 1 ppm [25]. It is an attractive candidate for many other emerging technologies, such as supercapacitors [26], light-emitting diodes (LEDs) [27], light-emitting electrochemical cells [7], solar cells [28, 29], artificial muscle [30, 31], and in enzyme logic switches [32]. Modern-day flexible organic LEDs utilize poly(2-methylxy-5-(2-ethylhexyloxy)-1,4-phenylenevinylene (MEH-PPV), which is used as an

excited state quencher in DNA sensors [33]. PAni thin film electrodes are responsible for charge separation in optically transparent supercapacitors which charge under illumination [26]. This photo-induced charging of PAni has also been demonstrated in organic photovoltaics when made into a sandwich structure with titanium dioxide and indium tin oxide (ITO). PAni's nanoporous structure was reported to be the most crucial element to its charge transport mechanism, due to its good interfacial coverage [26]. Poly(vinylalcohol)-emeraldine base (PVA-EB) composite films had been reported as respiratory sensors, due to the protonation of conjugated polymers by carbonic acid, which is formed by the adsorption of carbon dioxide onto solid-state acidic PVA surfaces in electrochemical transistors [34]. Emeraldine base has also been used as a halogen sensing material due to the spontaneous substitution of X_2 (X= F, Cl, Br, I) onto EB carbon atoms, followed by the protonation of EB-PAni imine-nitrogens with the resulting acid byproduct [35]. H_2 sensors [36] and biosensors based on horseradish peroxidase have also been engineered using PAni [37].
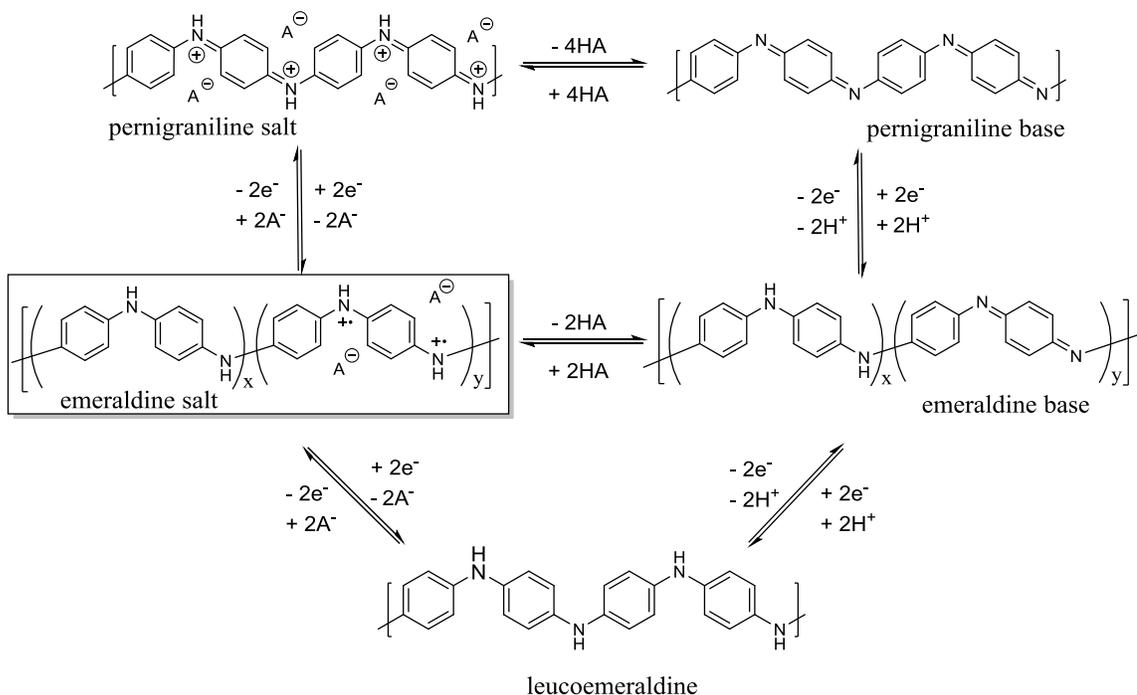
Figure 2.1: Redox and protonation transitions of PAni unit cells; unit cell ratio for emeraldine salt: x = 0.5 y = 0.5. [39, 40]

3

2.3 Mechanism of charge transfer in emeraldine salt

PAni can exist in several forms – as the green, metallic 10 S cm$^-$ emeraldine salt (ES) or as one of the insulating forms: the blue-colored emeraldine base (EB) form, the blue-violet pernigraniline salt (PS) and pernigraniline base (PB) forms, or the white leucoemeraldine (LE) form – all of which have conductivities of approximately 10^{-10} S cm$^-$ (ε: 3.35) [38]. A molecular representation of the doping-dedoping transitions of PAni is given in Fig. 2.1. PAni is a *p*-type organic semiconductor by which hole-injection occurs by tunneling or hopping events from drain to source [41]. Holes are injected into PAni-ES chains, typically at a 1 nm distance from the electrode [7].

After injection, holes propogate further into the polaron lattice. In doped conjugated polymers, charge delocalization is one-dimensional along the *π-band* – an electronic structure resulting in delocalized p_z orbitals of consecutive atoms. PAni-ES, which is a non-degenerate, hetero-atomic π-band conjugated polymer, undergoes one-dimensional charge delocalization due to electronic defects in the π-band in the form of quasiparticles on nitrogen atoms. The two quasiparticles responsible for conduction in PAni are the positive polaron and the positive bipolaron. The positive polaron in PAni consists of one neutral and one positive soliton on like nitrogen atoms [42, 43], whereas the bipolaron consists of localized like charges on adjacent nitrogen atoms [43]. Neutral solitons are breaks in conjugation characterized by a mid-gap state of ½ spin and no charge while positive solitons are responsible for a second mid-gap state having zero spin and positive charge. The combined spin and charge from the neutral and positive
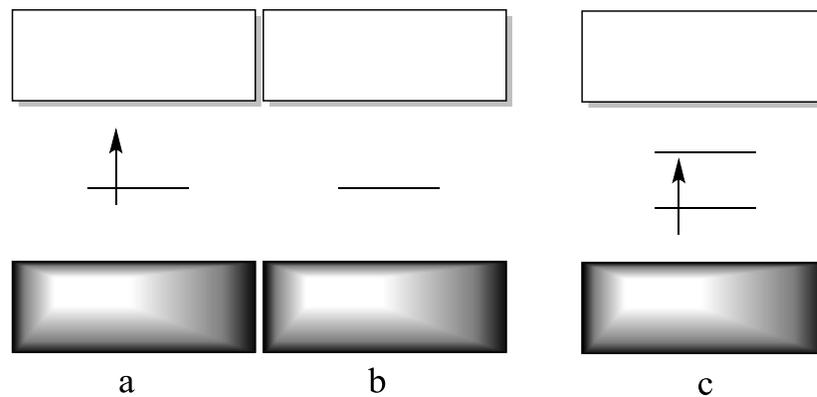
Figure 2.2: a) neutral soliton, b) positive soliton, c) positive polaron
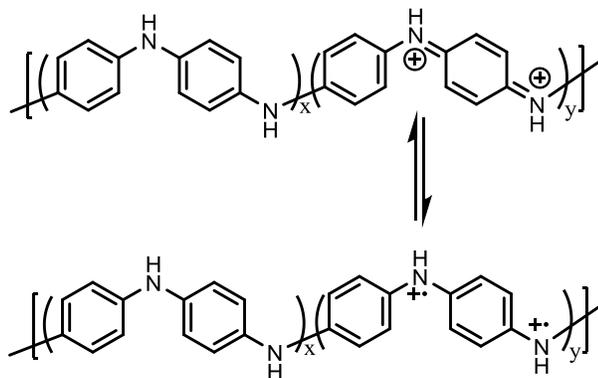
Figure 2.3: Structural confirmations of PAni-ES in the quinoid form (top) and benzenoid radical cation form (bottom)

solitons respectfully gives rise to electron-conjugated confirmations of the molecule, as drawn in Fig. 2.2. Bipolarons have not been observed *ex situ* in PAni-ES films upon protonation [39]. However, bipolarons have been indicated through a combination of spectroelectrochemical experiments at given onset potentials – a shift in C-H bending modes from globally aromatic to globally quinoid and a gradual diminishing of the Pauli susceptibility [40]. Additional evidence to support this claim is the intensity difference which arises at this onset voltage between insulating amine (1225 cm⁻) and charged amine (1255 cm⁻) Raman shifts – uncharged amines become much more prevalent with regard to positively charged amines, as imines are the charged species in bipolarons (Fig. 2.3) [40]. Bipolarons which form from protonation are rapidly relaxed to adjacent polarons and become delocalized [39]. The resulting polaronic lattice has two mid-gap defect states and is characterized by the presence of both charge and spin. Although it is not illustrated so in Fig. 2.2c, the higher energy defect – which is unoccupied – is optically indistinguishable from the conduction band [43].

As opposed to chaotic delocalizations in 3-D metals, PAni polarons rely on their interlocking into a polaron lattice for charges to exhibit enhancement of delocalization, prompting a quasi-metallic transport across molecules [7]. This charge-separated state in the donating molecule is stabilized by the conjugated polymer's highly polar environment [44]. In order for this charge-transport mechanism to occur in the first place, highly-linear aromatic chains must be in a matrix of interfacial aromatic molecules via π-stacking in a way which does not compromise the proximity of electron-conjugated regions [45-47]. Therefore, the anionic

stabilization of polaron quasiparticles, in tandem with π-stacking, enables ballistic transport across relatively long distances in PAni film.

2.4 The working principle of electrochemical transistors

When a conjugated polymer-electrolyte composite is interfaced with an ionic circuit, the resulting structure is known as an electrochemical transistor. The molecular benzenoid:quinoid ratio for doped PAni is 50%, and deviating from this ratio results in a gradual loss in
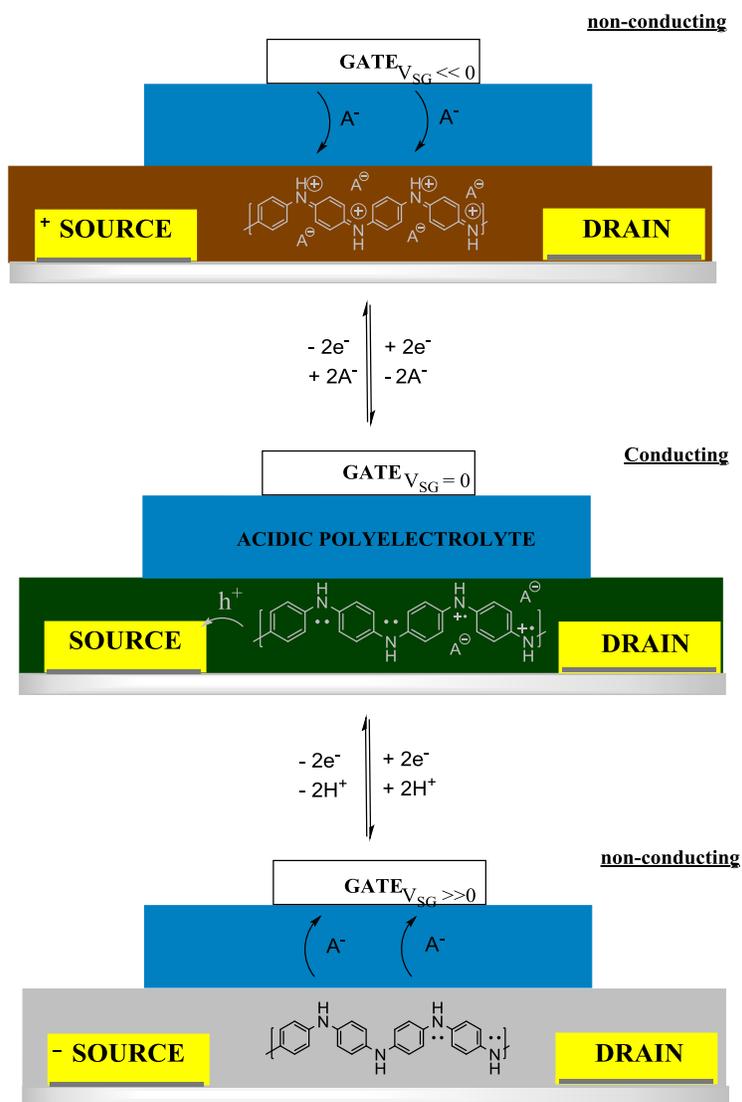
Figure 2.4: Schematic underlying the mechanism of electrochemical transconductance in PAni transistor

6

conductivity [48].   Dedoping of PAni can completely switch the source-drain on/off.
Cathodically polarizing PAni past the threshold for maximum optical polaronic absorption
causes the formation of excess bipolarons [40], leading to increasing local anion density causing
an increase of volume of the bulk polymer [7]. At greater potentials, this transition gives rise to
a largely insulating polymer film of PAni-PS (Fig. 2.4 top). Inversely, when anions are pulled
the from the semiconductor, excited states in PAni then thermally recombine and the material
becomes the electrically insultaing PAni-LE (Fig. 2.4 bottom). This anionic relaxation in the
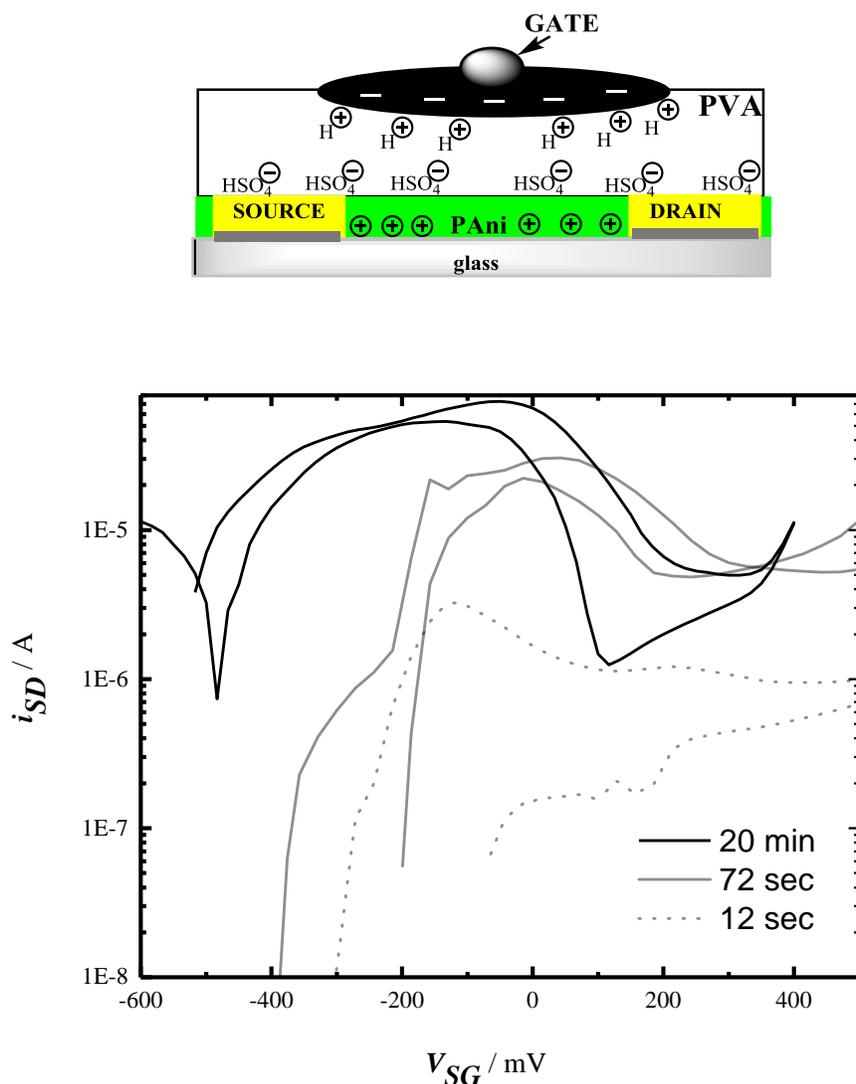
Figure 2.5: *Top)* Device architecture of a PAni electrochemical transistor not drawn to scale; characteristic dipole
relaxation with penetration of anions into PAni film. *Bottom)* visual representation of variation of hysteresis
between 12 s, 72 s, and 20 min anodically polymerized PAni electrochemical transistors

7

ionic circuit (Fig. 2.5a) is manipulated in electrochemical transistors. Since a reorganization of ions is necessary for the redox transformation of PAni, the metal-semiconductor transition is always characterized by some hysteresis (Fig. 2.5b) [7]. The various parameters of ECT fabrication which influence transistor response include electrolyte (composition, thickness, pH), temperature, humidity, and degree of percolation which is represented proportionately by electropolymerization time. In the semiconductor design process, one must make tradeoffs between force output and transconductance; a higher force output is achievable with increased film thickness, whereas increased film thickness slows down transconductance [7]. In contrast to field-effect transistors, electrochemical transistors operate at low voltages and can operate in either the Faradaic or non-Faradaic regime. In Faradaic operation in electrolyte-enzyme biosensors, for example, a redox mediator is quenched at the gate electrode, causing the modulation of source-drain current i_{SD} (Fig. 2.6) [7]. This is the working principle in electrolyte-gated field effect transistors (EGOFET) – a subcategory of ECTs [7]. Inversely, in non-Faradaic operation, ions migrate toward and away from the conjugated polymer film by an applied gate voltage, as previously described [7]. These are explicitly referred to as ECTs, and the work presented in this paper deals strictly with these devices. The enzymatic production of hydrogen peroxide by horseradish peroxidase is an established example of such product sensing by direct chemical oxidation [49]. Electrochemical displays, printed batteries, electrochemical paper labels, and sensors for construction and health-care have been put to the test on the market by firms such as Acreo and AGFA.
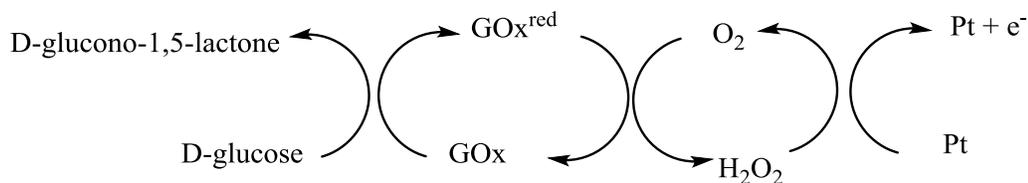
Figure 2.6: An example of a biosensor reaction scaffold which, in this case, dictates the Faradaic operation of a PEDOT:PSS ECT [7]

3. Fabrication procedure

The chemicals used in the fabrication were acetone (99.5%) and isopropanol (>95.5%) from VWR, Ammonium hydroxide aqueous solution (25%) and hydrochloric acid (37%) from Fischer Scientific, aniline (99.5), mowiol, and poly(4-styrenesulfonic acid) from Aldrich, hydrogen peroxide (30%) and ortho-phosphoric acid (85%) from Merck, sulfuric acid (95%) from Baker, Hellmanex III detergent from Hellma Analytics.

3.1 Substrate treatment

Glass slides were cut and fit into a substrate holder, which would hold the devices inside of a source-drain mask – source-drain electrodes were on the order of tens of microns. The glass slides were then inserted into a Telfon holder, which held the slides firmly with the backs of the slides - the sides with the numbers carved into them - all facing the same direction. The slide-containing holder was then submerged in a beaker containing acetone, so that all of the slides in the holder were immersed in liquid, and sonicated at room temperature for 15 minutes. Afterwards, the substrates were removed from the acetone-containing beaker and dried thoroughly with compressed air. Then, the slides were placed in a beaker containing isopropyl alcohol, once again so that all of the samples were immersed, and left to sonicate at 50°C for 15 minutes. Once the 15 minutes had elapsed, the samples and holder were thoroughly dried with compressed air and placed in a beaker of Hellmanex detergent, once again so that all samples were completely immersed, and let sonicate this time at 70°C for 15 minutes. After this step, the filled holder was then thoroughly rinsed with deionized water, as to remove the residual detergent on the slides and holder. Then, the filled holder was placed in a beaker containing deionized water, such that all samples were immersed, and let sonicate at room temperature for 15 minutes. Afterwards, the sample-containing holder was removed from the beaker and dried with compressed air.

3.2 Functionalization of the glass surface: base piranha

Next, the filled substrate-holder was submerged into a solution of RCA-1 basic etching solution and allowed to sonicate for 5 minutes. This solution was a 5:1:1 by volume mixture of deionized water, 25% ammonium hydroxide, and 30% hydrogen peroxide. This step was done in order to make the glass surface hydrophilic by the addition of hydrophilic functional groups to the glass surface.   After the 5 minutes of sonication had elapsed, the sample-containing holder was first rinsed with deionized water and dried with compressed air. Next, each sample was delicately removed from the holder, rinsed with isopropyl alcohol, then with water, dried with compressed air, and finally transferred into a petri dish, which was then sealed shut with paraffin wax film after all of the samples had been transferred.

3.3 Tooling

Tooling factors of 1.20 for Cr and 0.73 for Au had been calculated for the editors using actual nano-scale thickness values measured using a dektak profilometer and the following equation: $Tooling = \frac{Real\ thickness\ (determined\ by\ profilometer)}{Measured\ thickness\ on\ monitor}$. The tooling factor is necessary because the monitor cannot give accurate thickness values using only the density, δ, and acoustic impedance, Z, parameters, due to differences in granulation and adhesion among materials. Hence, this is a form of calibrating the thickness monitor. Tooling factors, as well as δ and Z values, were already determined and put into the monitor by the time these devices were being fabricated.

3.4 Physical vapor deposition

Physical vapor deposition (PVD) of thin-film electrodes is a critical step when the intent is to create percolated films. Since electrodes are 10 μm wide, this is a step which requires a great deal of sterility and environmental inertia. PVD was performed using a Leybold metal-induction chamber with a quartz crystal detector and monitor.   The evaporation chamber contained two separate PVD sources – one which would be used for Cr PVD and the other which would be

used for Au PVD. Cr is deposited before Au, since Au thin films delaminate off of glass but stick to Cr films. Each metal source was connected to its respective circuit via two copper cylinders separated by about 3 cm (Fig. 3.1). Each of the two metal sources was rendered ready for induction by the clamping of its respective tungsten entity – a Cr-plated W rod for the Cr source and a W boat for the Au source - to its designated circuit's copper cylinders. A gold pellet was placed onto the clamped tungsten boat, thus rendering the gold source complete.   The mask was made out of two circular sheet steel discs of equal area – one which contained six 2.5 cm x 0.9 cm cut-outs and one which contained a total of twenty-four source-drain cut-outs – aligned in groups of four under each substrate. The source-drain cutouts were distributed into six groups of four, overlapping four source-drain electrodes with each of the six substrate cutouts of
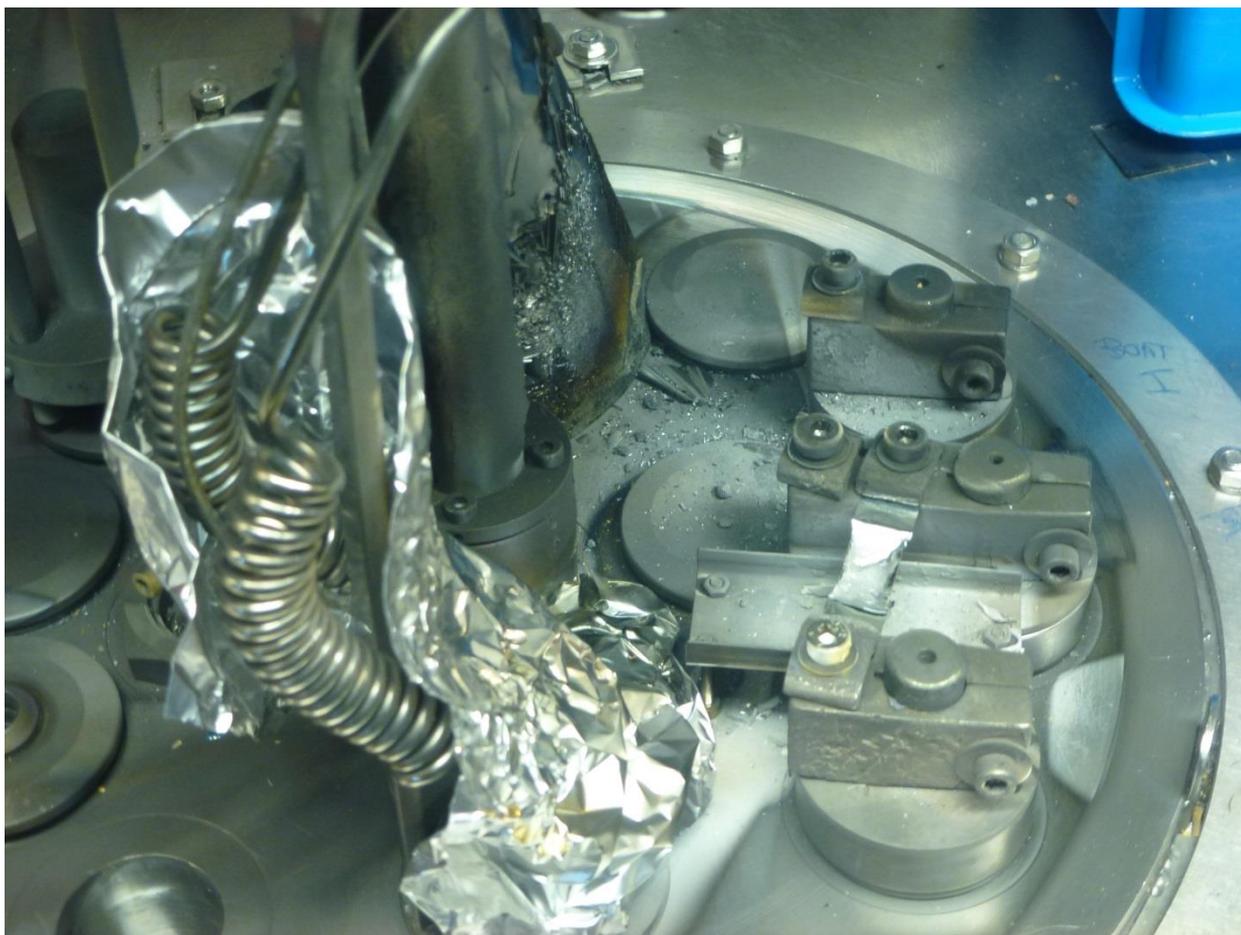

Figure 3.1: Photograph of the inside of the chamber for PVD

the first steel disc. After assembling, each of the six substrate holders of the first steel disc appeared to be masked with four soon-to-be source-drain electrodes – as well as a bar electrode which would not be utilized in this work – of the second steel disc. The mask was then immobilized onto a fixed ring-stand in the evaporation chamber using a paper-clip, such that the mask was sitting directly above and lying orthogonally to the metal sources underneath. The cleaned glass substrates were placed firmly in the mask's substrate holders, with the "front" ends facing downward toward the metal sources. Finally, the shutter which controlled the substrates' exposure to the metal sources was shut. The chamber was then sealed and evacuated, first by roughing the chamber from 1 bar to $1*10^{-2}$ mbar, followed by fine pumping down to $5*10^{-6}$ mbar. Once this 10^9 order of magnitude pressure decrease was achieved, the monitor was set to its designated "Cr-editor," which contained input density, $\delta = 7.20$ g cm^{-3}, and acoustic impedance, $Z = 28.94$ g cm^{-2}, parameters, as well as the tooling factor. Sixty-seven amps were applied to the Cr-source, corresponding to a deposition rate of 0.15 nm s$^-$. After depositing approximately 0.5 nm of Cr, the shutter was opened and the monitor was set to begin measuring the deposited Cr thickness. After the monitor had recorded 5 nm, the power was reduced from 67 A to 0 A. It is important to add that neither the shutter nor the pressure inside the chamber were adjusted, as to avoid nudging the substrates the least bit within the mask's substrate holders, thus keeping the 60-micron space between the S-D devoid of future Au. The monitor was then set to its designated "Au-editor." One hundred eighty-five amps were then applied to the Au-source, prompting a deposition rate which started at 0.7 nm s$^-$ and steadily increased by approximately 0.05 nm*s^{-2} ($\delta = 19.30$ cm^{-3}, $Z = 29.17$ cm^{-2}, tooling = 0.73). After 95 nm had been evaporated, the power was reduced to zero, followed by the flooding of the chamber. The six samples were then transferred delicately into a petri dish "front" facing up, and sealed with paraffin wax film.

3.5 Preparation of silver chloride pseudo-reference electrode

A section of Ag wire was connected to a Jaissle potentiostat, along with a Pt CE and a Pt RE and were submerged into a vial of 1.0 M HCl; Ag(s)|AgCl|HCl(1M)||HCl|H$^+$|H$_2$(g). Deposition of silver chloride was elicited via the following program: i. Roughing and cleaning [0.5, 0.1 V (SHE)], 10x, 10 mV s$^-$ ii. Deposition: (0.1 V, 120 s), (0.3 V, 600 s) iii. Rinse, air dry – the product is was noticeably darker silver chloride reference electrode (RE).

3.6 Preparation of monomer solution

Aniline was distilled using a Vigreux column from a mixture of aniline and nitrobenzene, via vacuum distillation at approximately 195° C. Although the original contaminated mixture was yellow, the mother liquor was brown and the distillate was clear corresponding to frations of nitrobenzene and aniline, respectively. The aniline was then stored in an inert Ar atmosphere. The 8 ml monomer solution was an aqueous solution of sulfuric acid (1.0 M, 0.426 ml, 0.78 g) and aniline (0.08 M, 58 μl, 59 mg), which precipitated briefly into anilinium bisulfate upon mixing before it readily dissolved. Anilinium bisulfate, unlike aniline, is a highly polar compound and does not undergo oxidation into nitrobenzene under ambient conditions.

3.7 Construction of electrochemical droplet cell housing

Since the Au working electrode (WE) consisted of two adjacent thin films atop a glass slide, innovative measures had to be taken in order to create an electrochemical cell where only the active channel area was in contact with the monomer solution. The immobilization of a tiny cross-section of a cylindrical rubber tube atop the source-drain active channel was first envisioned. Polydimethylsiloxane (PDMS) gel was used for its desirable adhesion to glass, its chemical inertness, and lack of permittivity. The PDMS "block" was formed by mixing together Dow Chemical's PDMS elastomer and curing agents in a 10:1 gravimetric ratio in a petri dish before placing on a heated surface or a furnace or oven at 80° C for 30 min. After being allowed to cool for 10 min, the PDMS was then ready to be punched directly with a circular hollow punch with a diameter of 2.5 mm. After punching four holes into the block overlapping with the four source-drain active channels, a scalpel was used to cut the four hole-containing block out of the petri dish, with caution being taken to cut the block small enough so that it does not hang off the glass substrate and narrow enough so as not to cover the source-drain terminals adjacent to each active channel. Then finally, the newly-cut PDMS block was lain onto the front side of a glass substrate, such that a Au source-drain active channel was exposed on the bottom of each of the four holes, rendering the electrochemical cell ready for assembly.

3.8 Electropolymerization of aniline

Electropolymerization of aniline was conducted inside of constructed wells with a volume of 15 µl which was constructed by punching holes out of the PDMS block. A silver chloride RE was used for the electropolymerization in order to monitor the actual potential between cathode and anode, which deviates from set potentials due to electrolytic resistance. However, its inclusion was not particularly necessary, considering that aniline will undergo anodic oxidation at electrical potentials beyond the second oxidation peak from the "before" portion of Fig 2.2, which are eight double-sweeps in monomer solution which took place initially on the fresh WE. From these eight sweeps, the onset of polymerization is depicted to be at potentials above
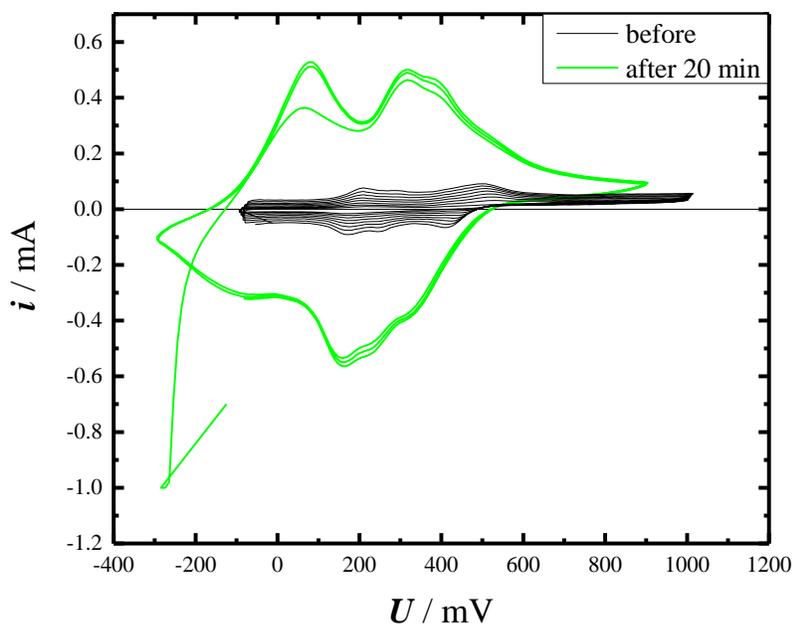
Figure 3.2: Cyclic voltammetry of of PAni(HSO$_4^-$) before (8 cycles) and after (1 cycle) a twenty minute anodic polymerization - using a holdvalue of 1000 mV in 1.0 M H$_2$SO$_4$ and 0.05 M aniline; These measurements as well as the polymerizations in between were carried out using a Pt CE, Ag|AgCl RE, and a WE consisting of two parallel coplanar Cr/Au thin film electrodes 20 mm long on glass with 60 µm inter-channel spacing

800 mV vs. Ag/AgCl. An electrical potential hold-value of 1000 mV vs. Ag/AgCl was used for all experiments. The assembled electrochemical cell (Fig. 3.3) consisted of the *active channel*

portion of the thin-film Au source-drain on the glass substrate as working electrode (WE) and approximately 20 µl monomer solution inside of the well (enough so that the solution protruded the top of the well-shaped cell), with the aforementioned RE, and a Pt counter electrode (CE) both submerged in the well's solution from above. Probes were magnetically mounted atop each of the two WE terminals (source and drain) and contacted together using alligator clips. The resistance across the wire connecting the two alligator clips was 0.1 Ω, thus rendering the two working electrodes slightly unequal anodes, according to Ohm's law. Both the CE and RE were wires and were mounted onto micro-probe stations. An electrical potential hold value of 1000 mV was applied using a Jaissle potentiometer to elicit electropolymerization. After electropolymerization, the source-drain was rinsed with 0.2 M HCl and then dried by blowing with compressed air. Hold times for electropolymerization varied among samples and will be specified in Section 4.6 in the results.
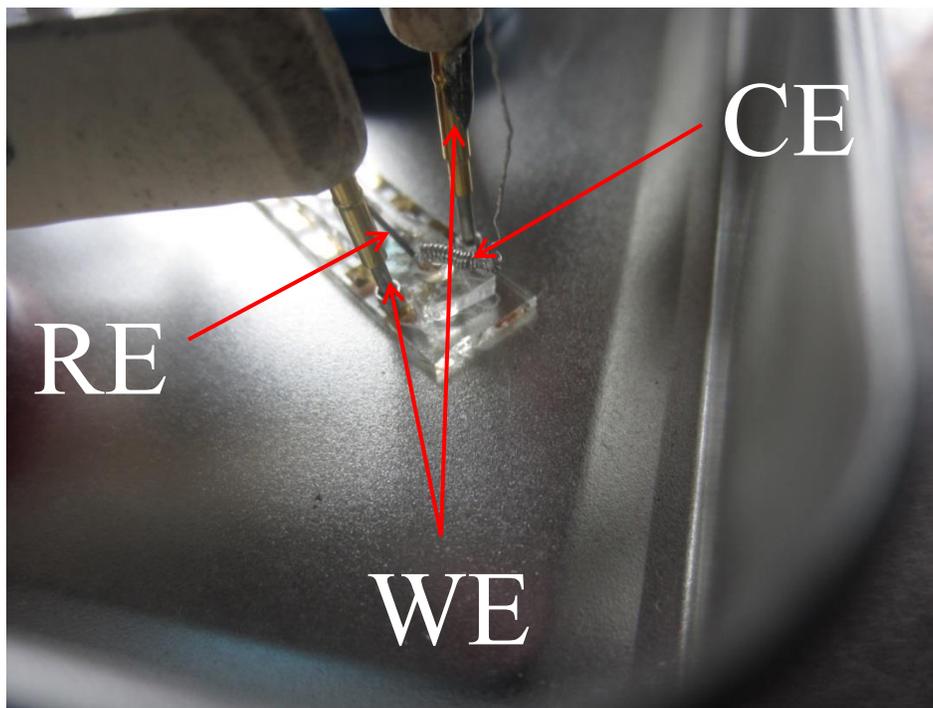
Figure 3.3: The 20 µl electrochemical cell used in the anodic polymerization of aniline

3.9 Polyelectrolyte deposition

For the preparation of sulfuric acid (SA) solid-state electrolyte, a 1.0 M amount was added to a 5% wt. polyvinyl alcohol (PVA) solution and stirred. A polystyrene sulfonic acid (PSSA) solid-state control electrolyte was made by adding 3.36 ml of 18% PSSA – corresponding to 1.19 M sulfonic acid monomers – in water to 0.64 ml water, creating a PSSA electrolyte with 1.0 M sulfonic acid monomers. It should be reiterated that this was not a 1.0 M solution of PSSA, but of sulfonic acid which was polymerized (MW of vinyl styrene sulfonic acid: 184 g/mol). Next, the solid-state electrolyte layer was deposited onto the device, either by spin-coating, drop-casting, or by gel-reservoir deposition in a PDMS well over the active channel. All devices – regardless of electrolyte composition and deposition method – were then allowed to dry for 2 h in ambient conditions. Once dried, the solid-state electrolyte layers in each of the devices were 4 μm, except for in Section 4.3 in the results, where thicknesses are specified with the corresponding data.

3.10 Gate electrode deposition

Using a #2 paint brush, liquid carbon black was dabbed onto a section of the dried solid-state electrolyte layers directly above and slightly laterally displaced from the active-channel (microscope image), except for the devices in Section 4.8 in the results, by which the specific gate architectures used are denoted with the corresponding data. Silver paste was then dabbed atop the carbon-painted areas, so as to increase the connectivity of the carbon to the parameter analyzer. The silver paste was more viscous than the diluted carbon. However, should the silver paste be less viscous, dilution with acetone could be advisable. The silver paste was let dry for 1 h, rendering the transistor ready for analysis.

4. Results and discussion

4.1 Dependence of percolated film thickness and resistance on hold-time of anodic potential value
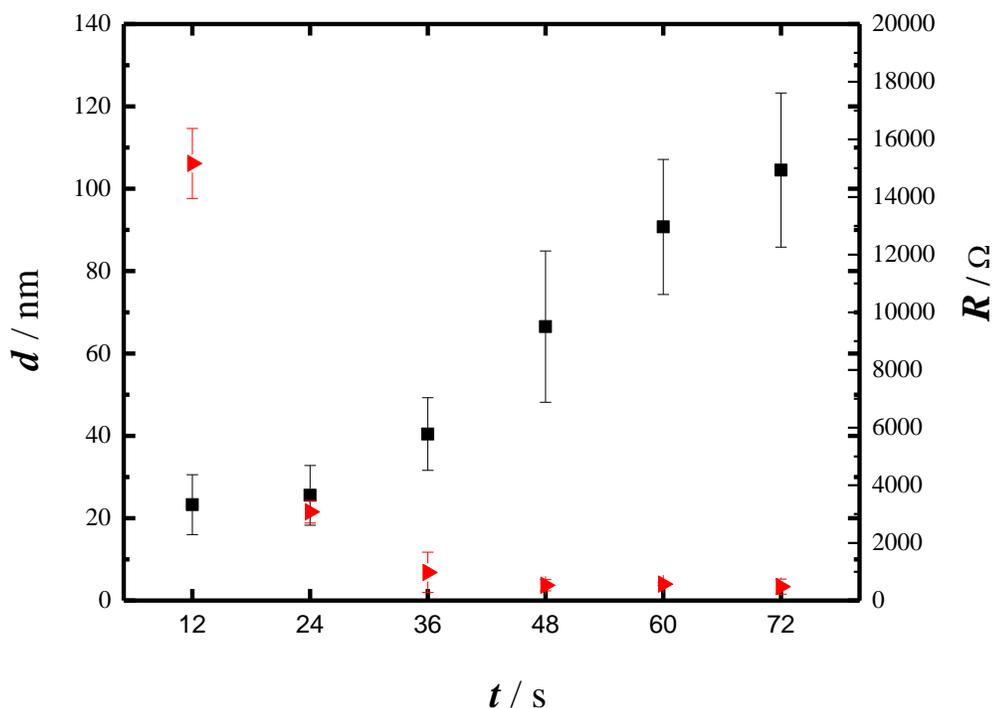
Figure 4.1: Time dependence of thickness d (squares) and resistance R (triangles) of electropolymerized PAni films

It came as quite a surprise that electropolymerized PAni on a hydrophilic glass surface, traversed over thirty microns laterally in a matter of nine to twelve seconds (Fig. 4.1), forming a percolated film between the lateral source and drains (displacement 60 μm). Films corresponding to electropolymerization times t_{EP} of 10 s, 16 s, and 40 s were investigated using a scanning electron microscope (SEM); the SEM images from Fig. 4.2a-d illustrate the transition from a partially percolated channel to a fully percolated one, as one can see a clear pale fissure in the dark regions in the channel in Fig. 4.2a that is a much less noticeable in Fig. 4.2d. This is a visual clue that by 10 s percolation is achieved. Furthermore, in Fig. 4.2b-e, one can see the progressive lateral percolation of the dark, uniform films at the edge of the active channel. Therefore, the gradual increase of film thickness depicted in Fig. 4.1 is attributed to higher

percolation within the channel. The dark portions of the channel film as depicted in these figures, therefore, are responsible for the electrical conductivity of the films, yet the formation of granules on the electrodes and active channel are steadfast accompaniments of this polymerization. As can be seen in Fig. 4.3a, the dark, percolating film becomes broader and enhances the conductivity of the film. The possible removal of granules from films electropolymerized forty-eight seconds would decrease the film thickness by an average value of 250% without affecting film conductivity. It is evident that additional percolation events which
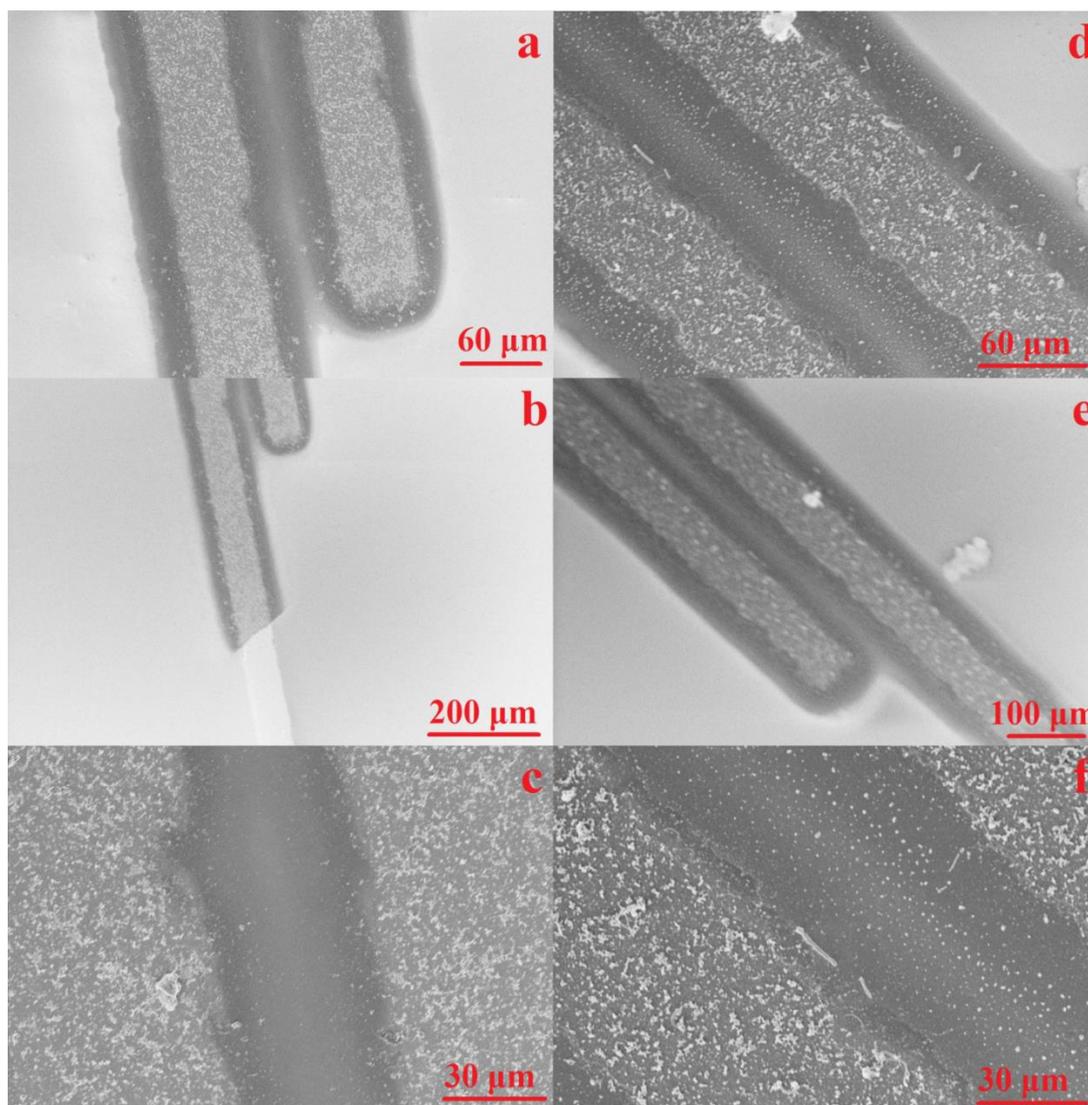
Figure 4.2: PAni thin films resulting from percolation after 10 s (a-c) and 16 s (d-f) of electrolysis

take place between the source and drain between 12 and 36 s are responsible for the exponential decrease in film resistance. As can be seen from Fig. 4.3a, these events have occurred extensively such that nano-film boundaries at 40 s are noticeably wider than those at 10 s or 16 s, and also there is no remaining fissure. With the resistance PAni films approaching a critical minimum at about 40 s, it can be concluded that the transparent, percolated PAni lamella relies solely on the degree of percolation for it to be a conductive entity. This is also exhibited in images in Fig. 4.4, whereby conductive nano-films are observable only as a light tint under 1000% magnification.
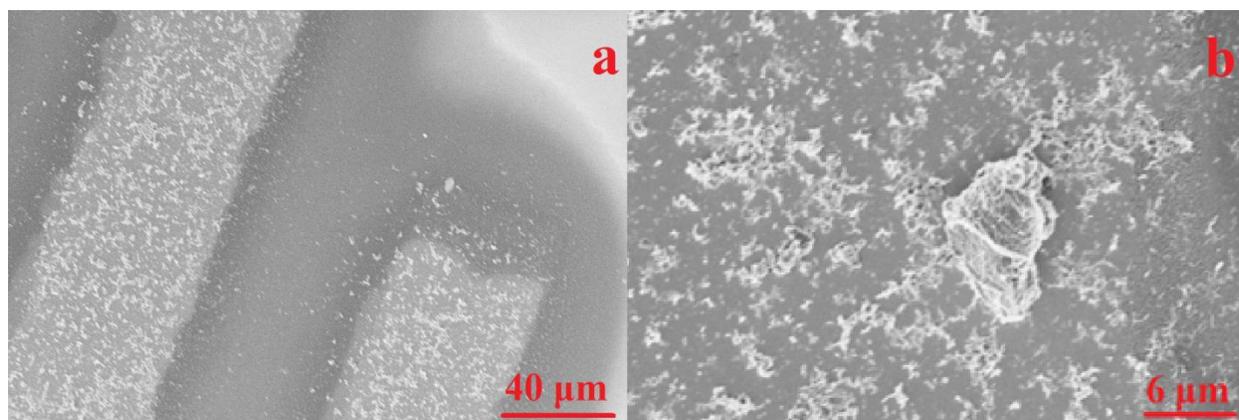
Figure 4.3: a) PAni thin-film, represented by the darkened regions surrounding the two finger-shaped electrodes, from interdigitated percolation after an application of oxidative bias on them coupled together lasting forty seconds, b) dense electropolymerized granule on the surface of a thin-film Au electrode
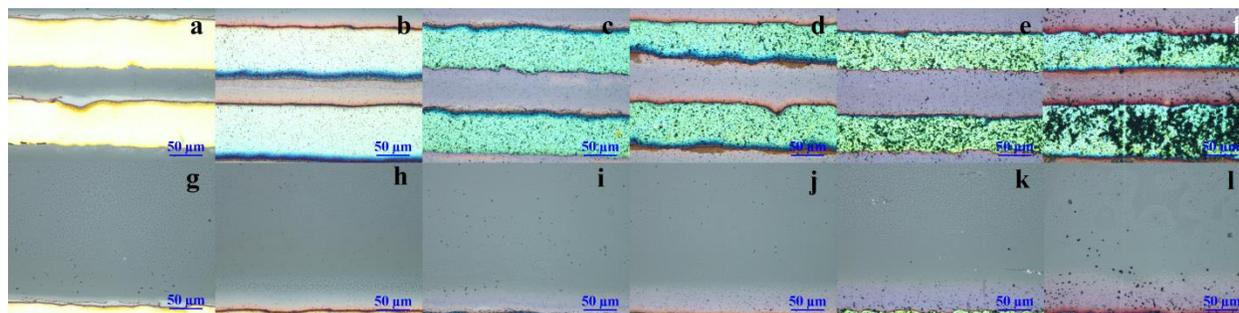
Figure 4.4: 400x magnified images of active channel films (*a-f*) and glass-electrode boundaries lateral to the active channel (*g-l*) – images correspond to different electropolymerization times at 1000 mV; *a,g*) 12 s *b,h*) 24 s *c,i*) 36 s *d,j*) 48 s *e,k*) 60 s *f,l*) 72 s

4.2 Coulometry of anodic film percolation

After making i vs. t plots for the anodic polymerizations conducted in Section 4.1, the total number of charge was calculated for each of them.   The areas under the curves were integrated with Origin 9.1G software. Each area value then underwent dimensional analysis to yield the total charge throughput in coulombs based on the integral relation between charge and current. In the I vs. t plot, as seen in Fig. 4.5, the discharge current at the onset of bias is due to dipolar relaxation of the electrolytes in solution, namely anilinium, bisulfate, and hydrogen nuclei, and it is relaxed after approximately 7 s. This is known as the displacement, or capacitative charging current. The current then increased over the next three seconds, reaching a local maximum at about ten seconds consistently. This is hypothesized to be an indicator of the first percolation of the PAni across the 60 μm channel separating the two Au electrodes, forming the first polymer links on the hydrophilic glass. Fig. 4.6 shows the evolution of film linkage and formation in the subsequent seconds during and after percolation.   Thereafter, as the film had continued to
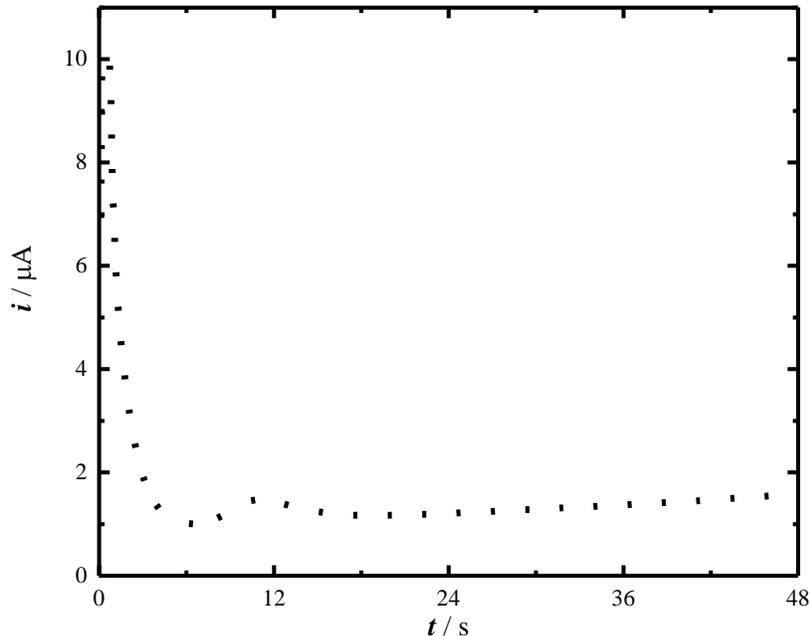
Figure 4.5: Current, i, vs. time, t, plot of electrochemical polymerization of aniline atop a hydrophilic glass surface using two Au thin-film anode fingers separated by 60 μm

percolate across the entire 2 mm length of the parallel electrodes in the following three to four seconds, the current had levelled off, with self-assembly of lamellar structure reaching an offset at about 18 s.

In the electrochemical cell, current passes from counter electrode through electrolyte to working electrode as anilinium ion radicals which propogate, yielding higher order oligomers by the mechanism illustrated in Fig. 4.7. On the working electrode, anodic oxidation of anilinium is the predominant reaction which takes place, and the produced electrons are injected into the Au electrodes as electrical current by the amperometric function of the potentiometer. The relationship between percolated film resistance and thickness versus charge in Fig. 4.8 shows a similar trend as the relationship versus electropolymerization time (Fig. 4.1).
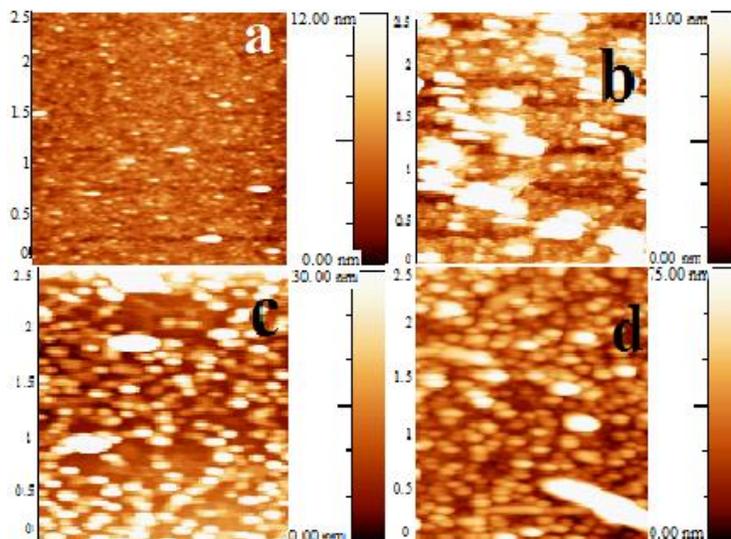
Figure 4.6: AFM images capturing changes in morphology at the fissure on a) 6, b) 12, c) 24, and d) 36 second-long percolated films
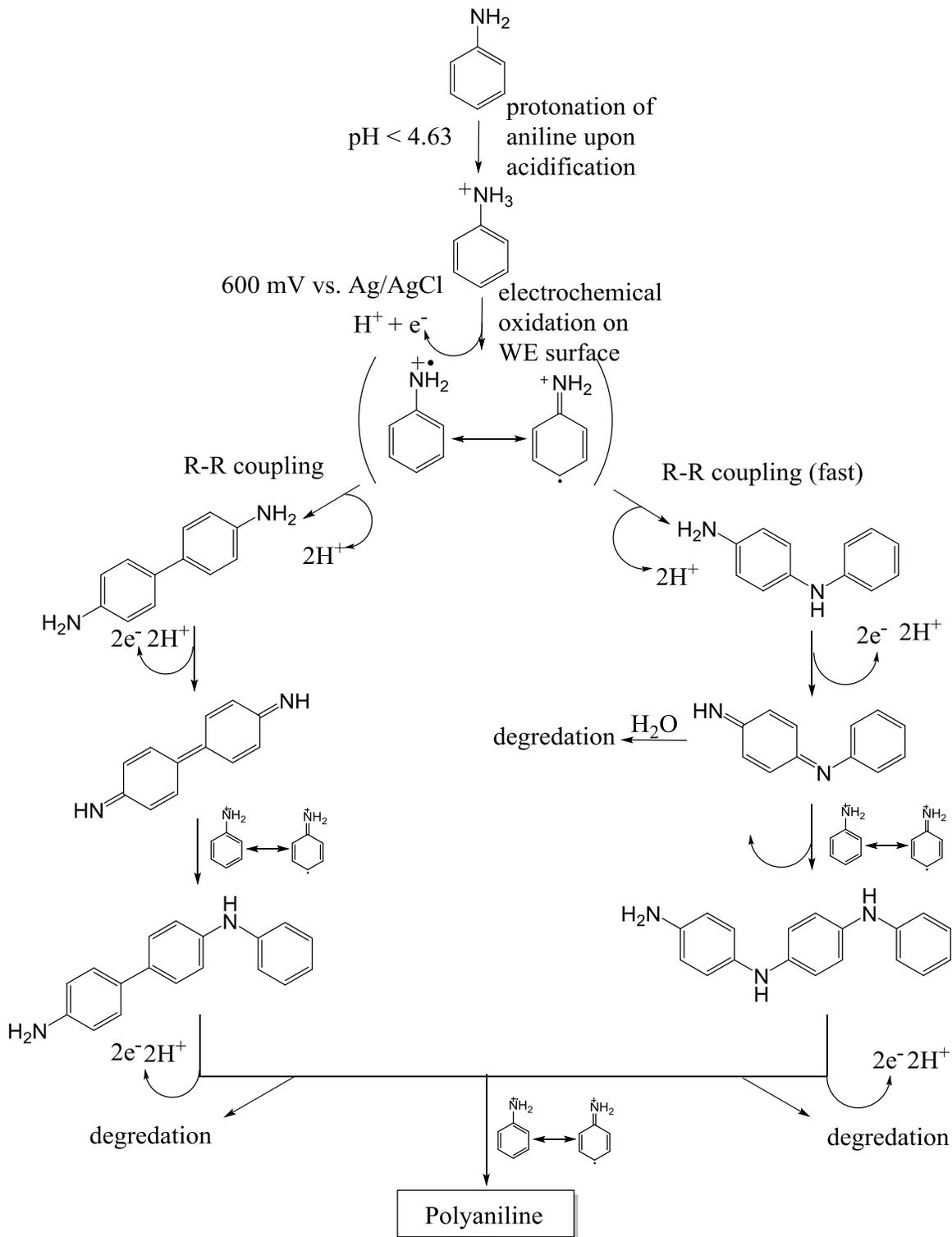
Figure 4.7: Mechanism of electrochemical polymerization of aniline [50]
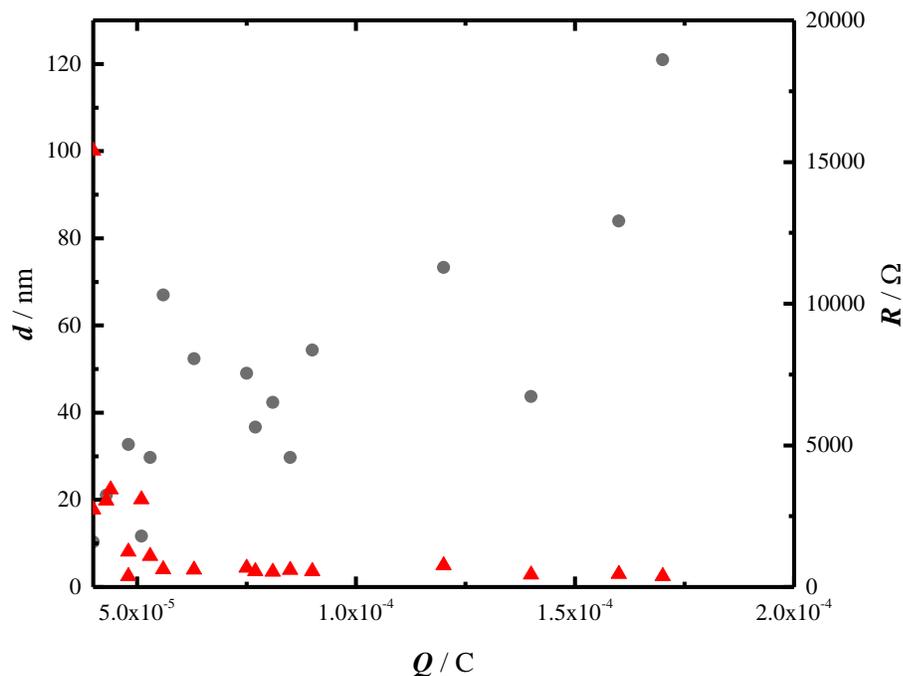
Figure 4.8: PAni film thickness, *d* (circles) and electrical resistance *R* (triangles) as a function of total charge, *Q*

AFM images were taken using a NanoScope IIIa scanning probe microscope from Digital Instruments. Mid-channel AFM images of percolated films are given in Fig. 4.6 which illustrate that percolation had continued to take place up to 36 s. The stagnation of film growth was conversely much more rapid in electrode-local regions of the channel as shown in Fig. 4.9.

It is evident here that electrode-local regions of the percolated film reached a stand-still at some point between 8-12 s, as the aspect ratios in figures Fig. 4.9c and 4.9d are more or less the same. The completion of a stage in lamellar evolution near the electrode is a determining factor in the minimizing of cross-channel resistance. This electrode-local PAni layer observed at 10 s no doubt plays a role in charge transport, however, not the major limiting role, which is the percolation and disappearance of fissure in the areas farthest from the WE.
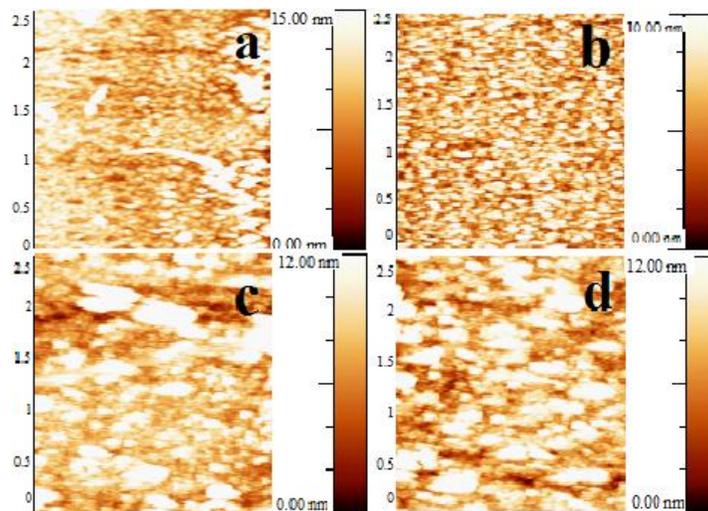
Figure 4.9: AFM images capturing changes in morphology on electrode-local regions of a) 4, b) 8, c) 12, and d) 16 second-long percolated films

4.3 Dependence of transconductance on electrolyte medium

Even though deciding upon a medium in the make-up of an electrochemical transistor may at first seem arbitrary, it turns out that it is a very important factor to consider, as different acids cause PAni to undergo varying degrees of doping [51]. Depending on the device operation that one wants, devices will be constructed utilizing a type of gel at a predetermined concentration and thickness. Voltage transfer characteristics of gel and aqueous solution electrolyte-based electrochemical transistors of equal ionic concentrations are illustrated in Fig. 4.10 (Table 4.1).
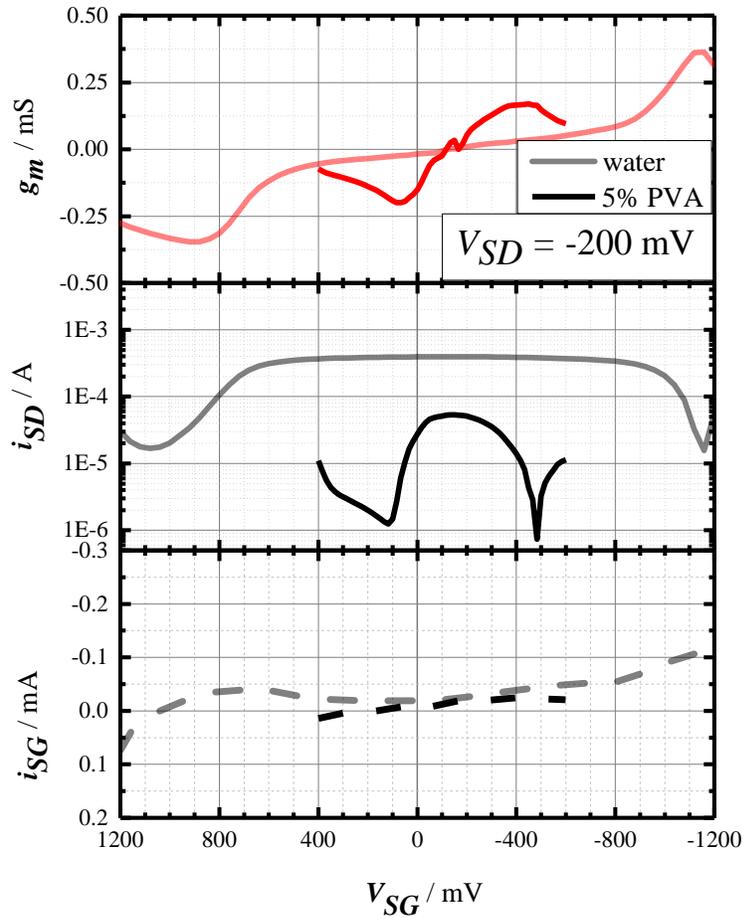
Figure 4.10: Voltage transfer curves of aqueous electrolyte vs. solid-state electrolyte; semiconductor electropolymerized 25 min; Pt foil gate for aqueous electrolyte-top gate atop 1 M H_2SO_4, silver paste gate painted on; 1.0 M H_2SO_4 5% PVA thin film polyelectrolyte

25

	Reductive transconductance					Oxidative transconductance				
	V_{TCD} / mV	V_{max} / mV	i_{TCD} / A	i_{max} / A	g_m / mS	V_{TCD} / mV	V_{max} / mV	i_{TCD} / A	i_{max} / A	g_m / mS
gel	66.7	-133.3	6.1E-06	5.4E-05	-0.24	-450	-133.3	4.31E-06	5.35E-05	0.16
liquid	920	-120	3.4E-05	3.9E-04	-0.35	-1160	-120	1.55E-05	3.94E-04	0.36

Table 4.1: g_m minima and maxima for polyelectrolyte and aqueous electrolyte-based electrochemical transistors; for each of PAni's two transconductances

Transistors using a solid-state electrolyte undergo comparable transconductances g_m with those using an aqueous electrolyte according to their voltage transfer characteristics. Based on this evidence, the assumption can be made suggesting that sulfate anions have a higher ionic mobility
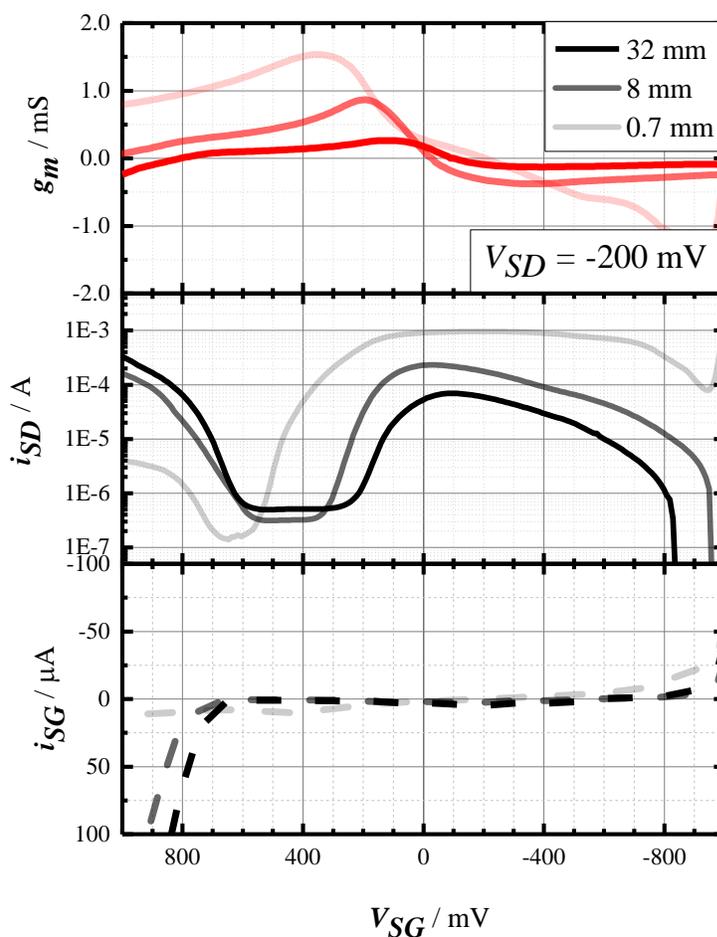
Figure 4.11: Voltage transfer curves of three different solid-state electrolyte thicknesses; all semiconductors electropolymerized 60 s; silver paste gate painted on; 1.0 M H_2SO_4 5% PVA thin film polyelectrolyte

	Reductive transconductance					Oxidative transconductance				
d_{gel} / nm	V_{TCD} / mV	V_{max} / mV	i_{TCD} / A	i_{max} / A	g_m / mS	V_{TCD} / mV	V_{max} / mV	i_{TCD} / A	i_{max} / A	g_m / mS
0.7	353.5	-202	-1.0E-04	9.55E-04	-1.9	-919.2	-202	-9.7E-05	9.6E-04	1.47
8	191.9	-30.3	3.8E-05	2.30E-04	-0.87	-363.6	-30.3	1.0E-04	2.3E-04	0.38
32	121.2	-90.9	1.4E-05	6.93E-05	-0.26	-393.9	-90.9	3.0E-05	6.9E-05	0.13

Table 4.2: g_m minima and maxima for ECTs of various polyelectrolyte thicknesses; for each of PAni's two transconductances

when in water as opposed to when in a PVA matrix. This is because, compared with the volume of the water electrolyte, the gel volume is much smaller. Therefore, a gel electrolyte-thickness versus g_m experiment was conducted; it was determined that increasing gel electrolyte-thickness is detrimental to the g_m by the results in Fig. 4.11 (Table 4.2).

The ionic circuit in electrochemical transistors, which consists of a gel electrolyte sandwiched between a conjugated polymer film and a painted-on carbon contact is a resistor and a capacitor in series (Fig 4.12). The resistor in this circuit denotes the electrolytic resistance of the gel electrolyte, which depends on the electroyte's ionic strength. At constant ionic strength, the difference in gel thickness is responsible for increasing the capacitive effect countering the dipole relaxations of ions. Therefore, it can be concluded that the spatial difference provided by the increase in thickness is responsible for an increase in ionic capacitance.
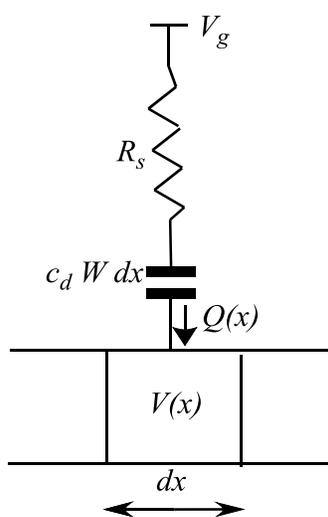
Figure 4.12: A conceptual diagram of an ionic circuit through which charges must be transferred to elicit modulation in an electrochemical transistor [7]

4.4 Effect of anionic species on transconductance

Besides thickness, another factor which greatly affects the capacitance of an ionic circuit is the mobility of ions in the gel matrix as well as the conjugated polymer matrix. Polyanionic chains are only able to interact with PAni at certain positions at the polyelectrolyte-semiconductor interface. The fact that any g_m *at all* was observed in this system is evidence that PAni exists only two-dimensionally. Furthermore, PSSA's less effective g_m as observed in Fig 4.13 (Table 3.3) is owing to the decreased ionic mobility of PSS⁻ molecules, in comparison to bisulfate which is a molecule consisting of only six nuclei [7]. During modulation by PSS⁻, polyanions bind to the percolated film in regions of lowest entropic cost, which means that PSS⁻
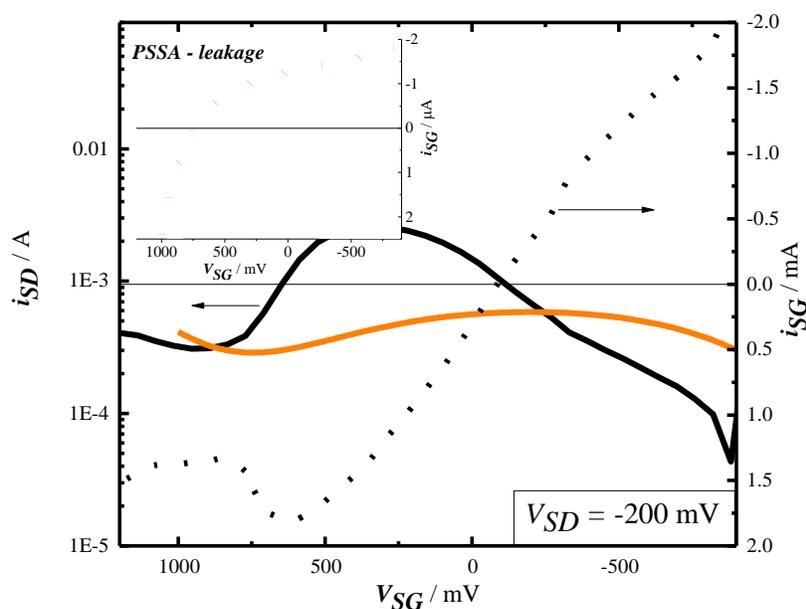
Figure 4.13: Voltage transfer curves of mobile, small-ion sulfate polyelectrolyte and immobile polyanionic PSSA polyelectrolyte; both semiconductors electropolymerized 60 s; silver paste gate painted on

	Reductive transconductance					Oxidative transconductance				
	V_{TCD}/ mV	V_{max}/ mV	i_{TCD}/ A	i_{max}/ A	g_m/ mS	V_{TCD}/ mV	V_{max}/ mV	i_{TCD}/ A	i_{max}/ A	g_m/ mS
SA	710.2	342.9	5.75E-04	0.00258	-5.5	-146.9	342.9	8.33E-04	0.00258	3.6
PSSA	587.9	-196	3.18E-04	5.85E-04	-0.3	-1000	-196	2.29E-04	5.85E-04	0.4

Table 4.3: g_m minima and maxima for PVA-SA and PVA-PSSA gel electrolytes; for each of PAni's two transconductances

molecules amass in areas of lowest PAni density at the fissure, i.e. the areas of lowest percolation. Therefore, the electronic-double layer capacitor formed by PSSA was sufficient for the formation of a polaron lattice to somewhat occur.

4.5 Effect of hydration on transductance

Another crucial design feature of the electrolyte medium in electrochemical transistors is the level of hydration [52]. PAni-based electrochemical transistors made by Wrighton in this publication demonstrate the dependence of g_m on hydration. A chemically polymerized PAni film, made by mixing stoichiometric amounts of aniline hydrochloride and ammonium peroxydisulfate in contact with the source-drain electrodes and the inner-channel was used for the transistor in Fig. 4.14 (Table 4.4). The "dry" transfer curve in the figure does not refer to the phosphoric acid gel electrolyte being dehydrated under Ar, but to it simply being in an ambient
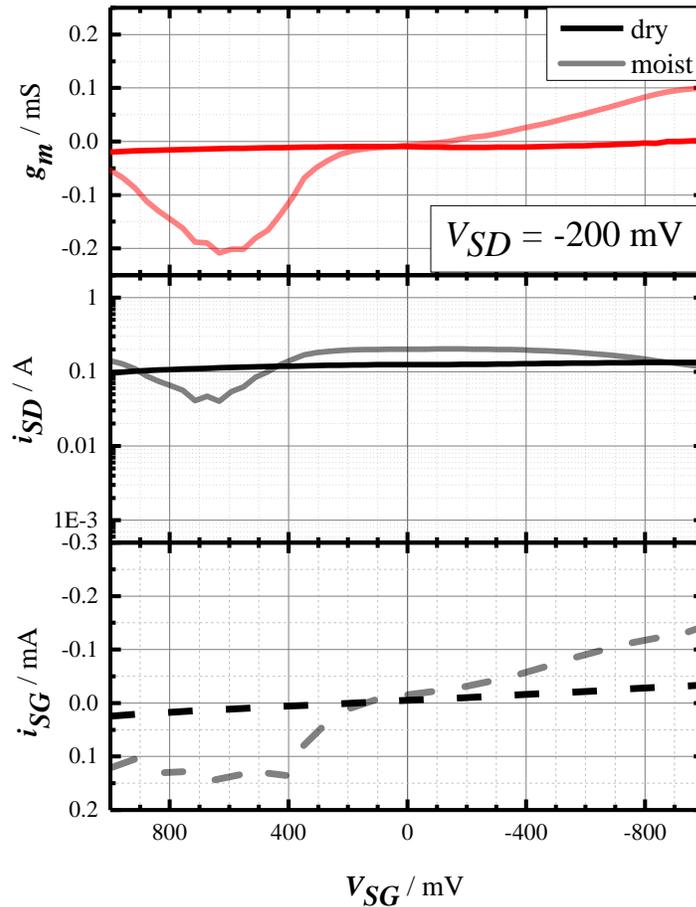
Figure 4.14: Voltage transfer curves of dry phosphate-electrolyte electrochemical transistor vs. immediately after steam exposure; semiconductor chemically polymerized 22 min; silver paste gate painted on; 1.0 M H_2SO_4 5% PVA thin film polyelectrolyte

	Reductive transconductance					Oxidative transconductance				
	V_{TCD} / mV	V_{max} / mV	i_{TCD} / A	i_{maxt} / A	g_m / mS	V_{TCD} / mV	V_{max} / mV	i_{TCD} / A	i_{max} / A	g_m / mS
dry	632.7	-142.9	3.99E-05	2.02E-04	-0.21	-1000	-142.9	1.17E-04	2.02E-04	0.01
moist	1000	-102	1.05E-04	2.32E-04	-0.12	-714.3	-102	1.82E-04	2.32E-04	0.08

Table 4.4: g_m minima and maxima of electrochemical transistors before and after exposure to steam; for each of PAni's two transconductances

atmosphere. After momentary exposure of the transistor's polyelectrolyte to hot steam, the modulation exhibited by the "immediately after moisture" transconductance took place. There was no decay of g_m, even two hours after the steam exposure. Hydration is evidently imperative for modulation of this system, which uses a 1 M phosphoric acid gel electrolyte. One molar
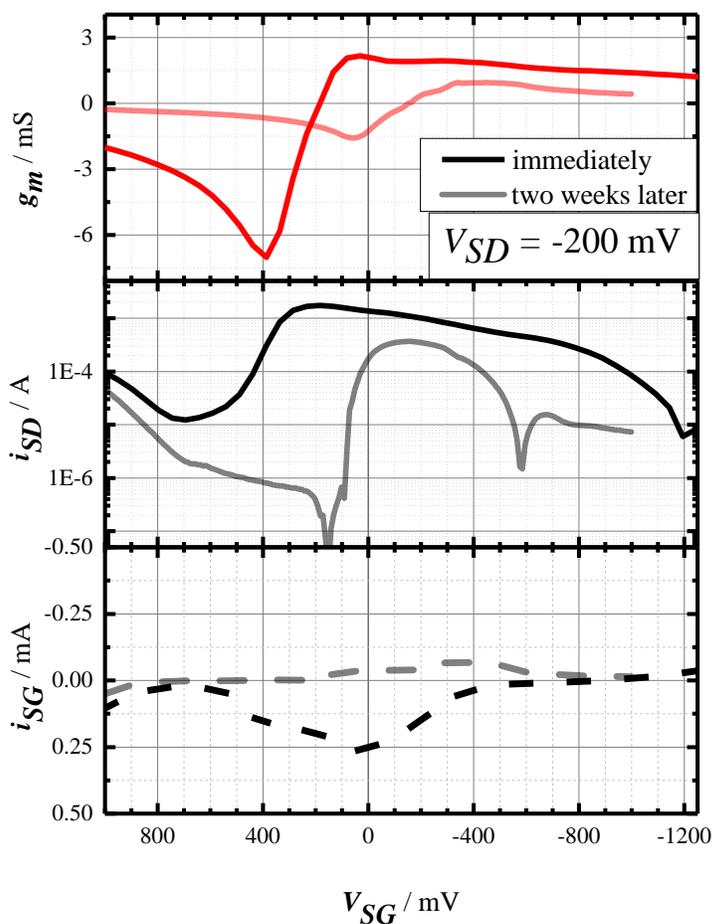
Figure 4.15: Voltage transfer characteristic illustrating g_m decay in a PAni(HSO$_4^-$) solid-state ECT over a two week period by comparing transconductance immediately after and two weeks after fabrication

phosphoric acid (pk_a 2.15) solution is pH 1.08 – much more acidic than the pk_a of PAni imino groups (pk_a 2.55) [43].   Therefore, in theory it is a sufficiently acidic electrolyte for maintaining a doped, protonated state of PAni. However, its anion concentration was much lower (0.084 M $H_2PO_4^-$) than that of 1 M sulfuric acid – which undergoes spontaneous dissociation into protons and HSO_4^-.   Nevertheless, hydration still plays a minor role in PVA-SA electrochemical transistors (Fig. 4.15).

4.6 Dependence of transconductance on electropolymerization time

As was proven in Section 4.1, albeit only using the first six 12 s intervals up to 72 s, the fact that longer anodic hold-value time increases percolation is further elaborated on in Fig. 4.16. When looking closely at g_m versus V_{SG}, a trend is observed in which transconductance maxima lie occur at increasingly higher potentials for samples with longer electropolymerization times; anions are undergoing maximum acceleration at more positive potentials for films with increasing percolation time. Various molecular forces such as van der Waals and London dispersion forces
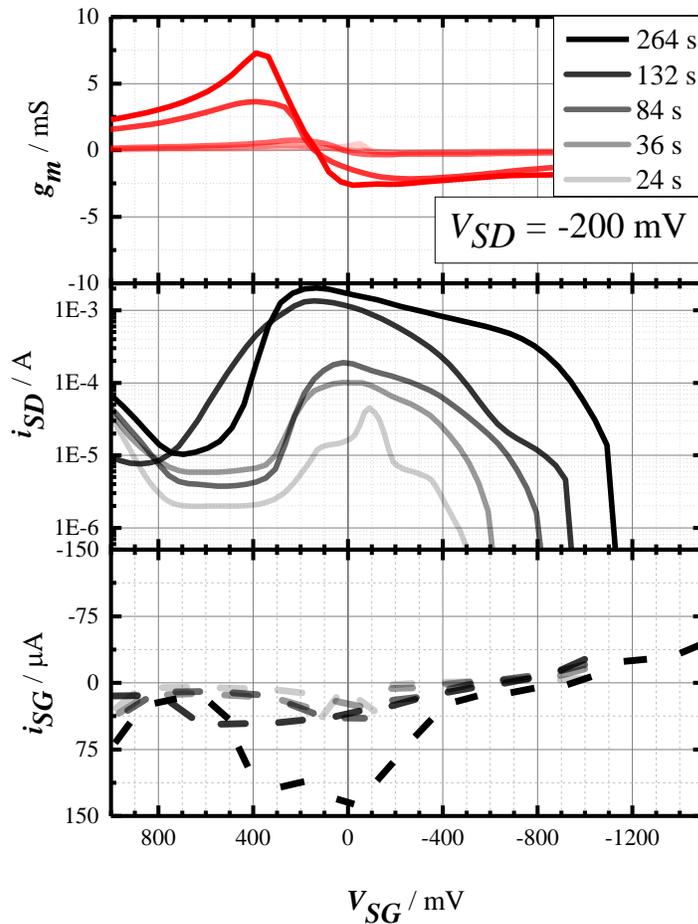
Figure 4.16: Voltage transfer curves of PAni transistors with various semiconductor electropolymerization times; silver paste gate painted on; 1.0 M H_2SO_4 5% PVA thin film polyelectrolyte

t_{EP} / s	Reductive transconductance					Oxidative transconductance				
	V_{TCD} / mV	V_{max} / mV	i_{TCD} / A	i_{max} / A	g_m / mS	V_{TCD} / mV	V_{max} / mV	i_{TCD} / A	i_{max} / A	g_m / mS
252	387.8	132.7	1.79E-04	0.00204	-7.3	-20.4	132.7	1.64E-03	2.04E-03	2.6
132	387.8	142.9	4.52E-04	0.00134	-3.6	-265.3	142.9	4.60E-04	1.34E-03	2.2
84	224.5	20.4	3.52E-05	1.89E-04	-0.8	-102	20.4	1.47E-04	1.89E-04	0.3
36	265.3	20.4	1.79E-05	1.01E-04	-0.3	-428.6	20.4	1.88E-05	1.01E-04	0.2
24	-50.5	-90.9	2.61E-05	4.49E-05	-0.5	-171.7	-90.9	1.20E-05	4.49E-05	0.4

Table 4.5: g_m minima and maxima for various semiconductor electropolymerization times; for each of PAni's two transconductances

must be accountable for this delay when dealing with thicker films. Somehow, dissociation of anions from the lamellar structures of the film upon dipole relaxation is slower. Layer-by-layer dedoping of thicker films may have given rise to the delays, with anions dissociating from compact nano-layers in a "please exit the movie theater from the entrance"-type fashion, rather than scattering past a wall of compact anions in the surrounding. This process can be compared to squeezing a big sponge full of water into a compact box and observing an increase in the potential energy needed to give the water maximum acceleration out the sponge with increasing sponge thickness.

4.7 Dependence of transconductance on scan rate

The frequency of operation for a given transistor will greatly influence its niche. [52]   With regard to frequency, Wrighton was troubled that at 100 Hz, amplification dropped drastically to the break-even point of power gain vs. frequency.   A transfer curve portraying the trend of transconductance decay as a result of increasing scan rate is illustrated in Fig. 4.17. (Table 4.6)
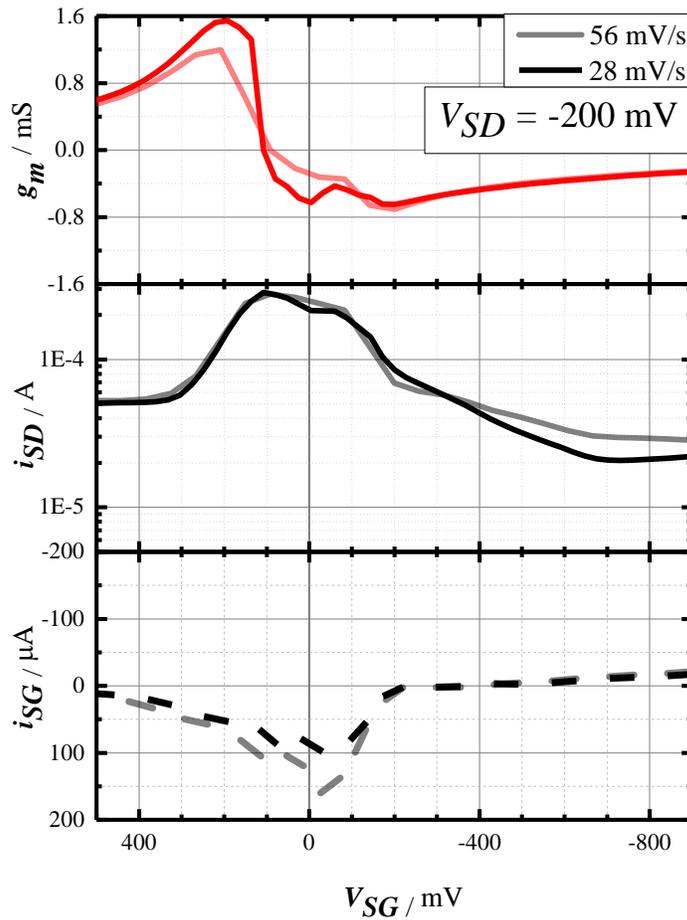
Figure 4.17: Voltage transfer characteristics of an electrochemical transistor at different scan rates; electropolymerized 60 s; silver paste gate painted on; 1.0 M H_2SO_4 5% PVA thin film polyelectrolyte

v / mV s⁻	Reductive transconductance					Oxidative transconductance				
	V_{TCD} / mV	V_{max} / mV	i_{TCD} / A	i_{max} / A	g_m / mS	V_{TCD} / mV	V_{max} / mV	i_{TCD} / A	i_{max} / A	g_m / mS
56	208.3	91.7	1.36E-04	2.76E-04	-1.2	-200	91.7	6.91E-05	2.76E-04	0.7
28	192	108	1.55E-04	2.85E-04	-1.6	-200	108	8.50E-05	2.85E-04	0.7

Table 4.6: g_m minima and maxima after increasing scan rate v by factor of two; for each of PAni's two transconductances

When electrochemical transistors undergo quick voltage sweeps, the resulting g_m is proportionately minimized, showing how g_m is indeed inversely proportional to modulation frequency.

4.8 Effects of gate connectivity on transconductance

Fig. 4.18 gives transfer curves of several different gate architectures. The design of the gate might seem like the most trivial. However, it is important that gates always be big for a strong coupling between source-drain current i_{SD} and gate voltage V_{SG} [7]. Moreover, increased
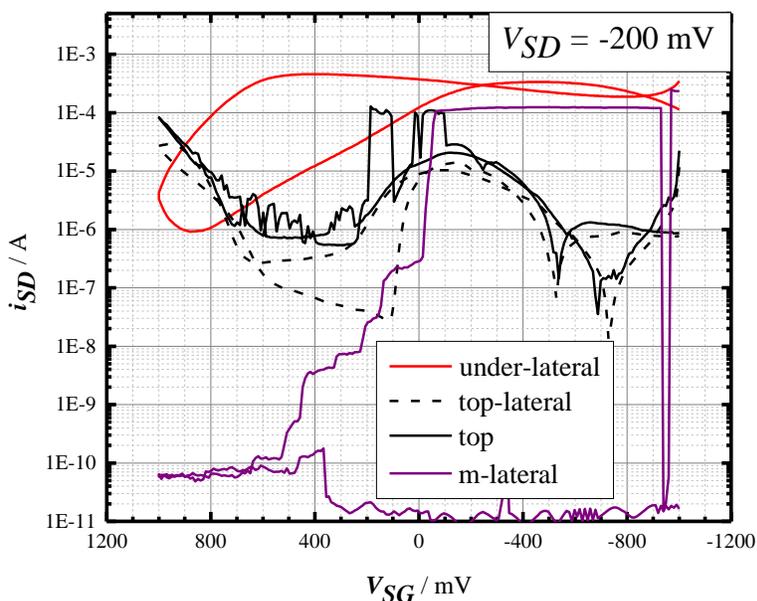
Figure 4.18: Voltage transfer characteristics for various gate architectures; all semiconductors electropolymerized 60 s; silver paste gate; 1.0 M H_2SO_4 5% PVA thin film polyelectrolyte

distance between gate and channel also decreases coupling due to the increase in necessary path length for dipolar relaxation to stabilize the channel material. Fig. 4.18 shows identical transconductance between gates directly on top and on top perpendicularly offset to the channel by 2 mm. Lateral gate electrochemical transistors functioned much slower because the gate's surface area facing the channel was very much less than the aforementioned two top-gate architectures, thus greatly lessening modulation. Lastly, an attempt was made at contacting a microscopic fleck of silver paste resting on the gel and it produced the transfer curve titled *µ-gate*. With the gate sometimes and sometimes not being coupled to the ionic circuit, PAni was revealed not to equilibrate automatically back to its default state. Another transfer curve in Fig. 4.19 shows a more pristine example of this memory capability.
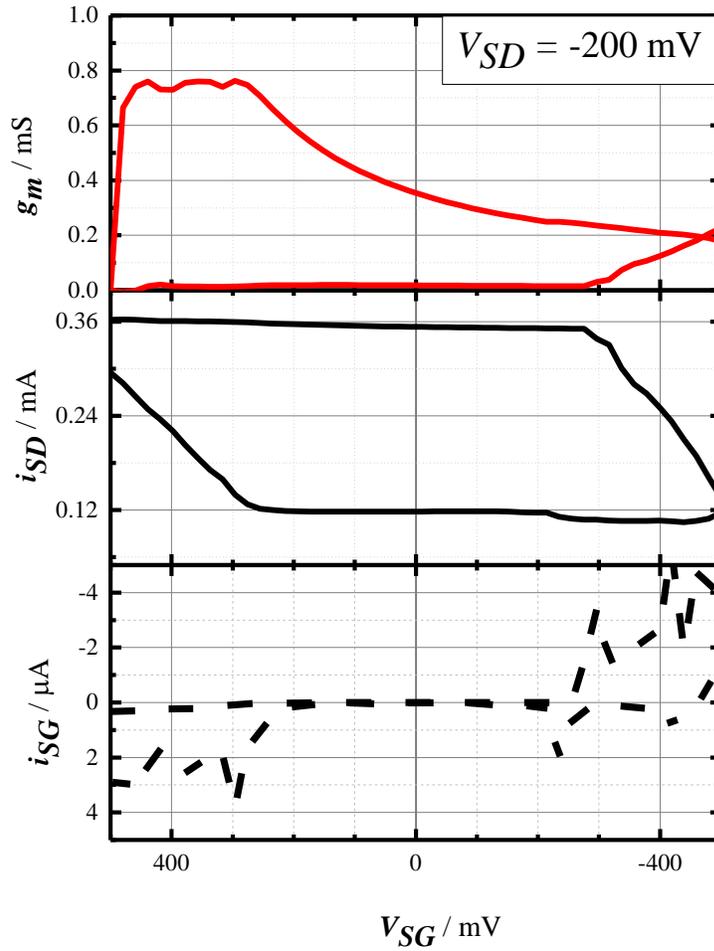
Figure 4.19: Voltage transfer charateristic with gate connectivity only featured in between -200 mV and -500 mV and again between 200 and 500 mV; semiconductor electropolymerized 60 s; silver paste-gate painted on; 1.0 M H_2SO_4 5% PVA thin film polyelectrolyte

Reductive transconductance					Oxidative transconductance				
V_{onset} / mV	V_{offset} / mV	i_{onset} / A	i_{offset} / A	g_m / mS	V_{onset} / mV	V_{offset} / mV	i_{onset} / A	i_{offset} / A	g_m / mS
-459.2	-500	0.00019	0.00014	-1.3	295.9	500	0.00014	0.0003	0.8

Table 4.7: g_m minimum and minimum in binary switching of memristor; for both oxidative and reductive transconductances

5 Conclusion

Although the method of film fabrication in this paper was a success, further considerations should be made in its possible optimization. Besides decreasing π-band protonation levels from unity to 0.5 [48], PAni's low intermolecular electronic overlap also needs to be accounted for. PAni's solvating groups have been proven to act as sidechains which, despite their pivotal role in polaron stabilization, perturb outer-sphere delocalization of charge carriers. Although π-stacking has been rather optimized in this fabrication, smaller anions of strong acids could be tested to increase interchain overlap[48].

Another point lies in the dimensionality of transport in these films. Conventionally with solution cast films of PAni, surfactant acids such as camphor sulfonic acid (CSA) have been used for doping, due to their enhanced magnetic susceptibility with respect to $PAni(SO_4^{2-})$ - with charge localization lengths on the order of 100 Å for CSA-doped PAni films by virtue of their enhanced intramolecular interactions [41]. Surfactants may not be necessary with this setup, however, as solution-cast films of tetraaniline nanofibers using HNO_3, H_2SO_4, $HClO_4$, and HCl dopant acids have been found to have a two-fold increase in conductivity compared to those of the best known higher-order PAni films [53]. Tetraaniline doped with H_2SO_4 has shown a flower-like nano-structure [53]. It is possible that the self-assembly from bridged-anode percolation involves similar three-dimensional pedal structures which undergo inter-mingling.

In this paper, despite producing efficient and conductive films without surfactants, it is not clear exactly *how* ordered films are. It would be worthwhile to see if incorporation of a surfactant acid into the monomer mixture would eliminate any existing defects in the molecular structure as it does in solution cast polymer films. This could be done using ECTs by implementing diagonal source and drain on a pre-percolated film. Doing so would determine the existence of anisotropy in mesoscale charge localization for these films. Furthermore, limiting the surface area of the WE to only the lateral portions by the addition of an insulating layer on the top of source and drain via PVD of an insulator could lead to more pristine lamellar structures with higher uniformity. Preventing granulation can help keep films optically transparent, while the incorporation of multiple transparent lamellar structures would increase charge density to practical amounts. Once percolated, these films could have the capacity to be

mechanically removed from their original anode bridge and adhered to other thin layers. Ultrathin films on the order of tens of nanometers thick can be pulled off of arrays according to sources [54, 55].

6 Summary

Bridged anode percolation yields PAni lamellae on glass with outstanding conductivity which cannot be achieved by solution casting. The evolution of cross-channel percolation, mid-channel granulation, and granular, nano-porous structure evolution on electrodes were observed by scanning electron microscopy (SEM) and atomic force microscopy (AFM). As can be seen from comparing dectac, SEM, and AFM topographies with resistance vs. time plots, the large PAni granules which give films opaque character and color are not important to film conductivity. With the electrochemical transistors used in this work, transconductance is optimized almost instantly after full percolation, yielding an aligned, conductive, transparent, and nanoscale lamellar film, whose metallic behavior has no dependence on growth in the z-direction; the optically transparent film thin films of thicknesses on the order of 50 nm work as good as thick-films (>1 μm). The PSSA solid-state electrolyte electric double-layer capacitor field-effect transistor had a very broad transconductance because polyanionic chains cannot penetrate the PAni interface, thus making charge injection into the PAni film feasible only where the solid-state electrolyte is bordering the PAni-electrode interface. Capacitive effects of gel and gate configuration were also explored. Finally, PAni electrochemical transistors had shown a memoristic capability.

Bibliography

[1] H. Zollinger, Color Chemistry: Syntheses, Properties, and Applications of Organic Dyes and Pigments Third. *Verlag Helvetica Chimica Acta AG Zurich, Switzerland*, revised edn, **2003**

[2] A.G. Lebed, The Physics of Organic Superconductors and Conductors. *Springer-Verlag Berlin Heidelberg*, **2008**

[3] P. Bernier, G. Bidan, S. Lefrant, Advances in Synthetic Metals: Twenty Years of Progress in Science and Technology. *Elsevier Science Lausanne, Switzerland*, 1st edn, **1999**

[4] Ho H, Leclerc M; Optical Sensors Based on Hybrid Aptamer/Conjugated Polymer Complexes, *J. Am. Chem. Soc.* **2004**, *126(5)*, 1384-1387

[5] Katz E, Willner I; Probing Biomolecular Interactions at Conductive and Semiconductive Surfaces by Impedance Spectroscopy: Routes to Impedimetric Immunosensors, DNA-Sensors, and Enzyme Biosensors, *Electroanalysis*. **2003**, *15(11)*, 913-947

[6] Gorou A, Noma T, Habu H, Yasumori I; Pyruvate Sensor Based on Pyruvate Oxidase Immobilized in a Poly(mercapto-*p*-benzoquinone) Film, *J. Electroanal. Chem.* **1999**, *464(2)*, 143-148

[7] J. Leger, M. Berggren, S. Carter, Iontronics: Ionic Carriers in Organic Electronic Materials and Devices. *CRC Press London*, **2010**

[8] Drury CJ, Mutsaers CMJ, Hart CM, Matters M, de Leeuw DM; Low-Cost All-Polymer Integrated Circuits, *Appl. Phys. Lett.* **1998,** *73(108)*, 108-110

[9] Tseng RJ, Baker CO, Shedd B, Huang J, Kaner RB, Ouyang J, Yang Y; Charge Transfer Effect in the Polyaniline-Gold Nanoparticle Memory System, *App. Phys. Lett.* **2007**, *90(053101)*, 1-3

[10] Reeves BD, Grenier CRG, Argun AA, Cirpan A, McCarley TD; Spray Coatable Electrochromic Dioxythiophene Polymers with High Coloration Efficiencies, *Macromolecules*. **2004**, *37(20)*, 7559-7569

[11] Shaheen SE, Brabec CJ, Sariciftci NS, Padinger F, Fromherz T, Hummelen JC; 2.5% Efficient Organic Plastic Solar Cells, *Appl. Phys. Lett.* **2001**, *78(6)*, 841-843

[12] Tang CW; Two-Layer Organic Photovoltaic Cell, *Appl. Phys. Lett.*, **1986**, *48(2)*, 183-185

[13] Graetzel M; Dye-Sensitized Solar Cells, Journal of Photochemistry and Photobiology C: *Photochem. Rev.* **2003**, *4(2)*, 145-153

[14] Guenes S, Neugebauer H, Sariciftci NS; Conjugated Polymer-Based Organic Solar *Cells*, *Chem. Rev.* **2007**, *107(4)***,** 1324-1338

[15] Glowacki ED, Irimia-Vladu M, Kaltenbrunner M, Gasiorowski J, White MS, Monkowius U, Romanazzi G, Suranna G, Mastrorilli P, Sekitani T, Bauer S, Someya R, Torsi L, Sariciftci NS; Hydrogen-Bonded Semiconducting Pigments for Air-Stable Field-Effect Transistors, *Adv. Mater.* **2013**, *25(11)*, 1563-1569

[16] Andreev A, Matt G, Brabec CJ, Sitter H, Badt D, Seyringer H, Sariciftci NS; Highly Anisotropically Self-Assembled Structures of para-Sexiphenyl Grown by Hot-Wall Epitaxy, *Adv. Mater.* **2000**, *12(9)*, 629-633

[17] Padinger F, Brabec CJ, Fromherz T, Hummelen JC, Sariciftci NS; Fabrication of Large Area Photovoltaic Devices Containing Various Blends of Polymer and Fullerene Derivatives by Using the Doctor Blade Technique, *Opto-Electron. Rev.* **2000**, *8(4)*, 280-283

[18] Kanazawa KK, Diaz AF, Geiss RH, Gill WD, Kwak JF, Logan JA, Rabolt JF, Street GB; 'Organic Metals': Polypyrrole, a Stable Synthetic 'Metallic' Polymer, *J.C.S. Chem. Comm.* **1979**, *14*, 854-855

[19] Hong W, Xu Y, Lu G, Li C, Shi G; Transparent Graphene/PEDOT–PSS Composite Films as Counter Electrodes of Dye-Sensitized Solar Cells, *Electrochem. Commun.* **2008**, *10(10)***,** 1555-1558

[20] Ellis DL, Zakin MR, Bernstein LS, Rubner MF; Conductive Polymer Films as Ultrasensitive Chemical Sensors for Hydrazine and Monomethylhydrazine Vapor, *Anal. Chem.* **1996**, *68(5)*, 817-822

[21] Kudoh Y, Akami K, Matsuya Y; Solid Electrolytic Capacitor with Highly Stable Conducting Polymer as a Counter Electrode, *Synth. Met.* **1999**, *102(1-3)*, 973-974

[22] Sakamoto S, Okumura M, Zhao Z, Furukawa Y; Raman Spectral Changes of PEDOT-PSS in Polymer Light Emitting Diodes Upon Operation, *Chem. Phys. Lett.* **2005**, *412(4-6)*, 395-398

[23] Khodagholy D, Curto VF, Fraser KF, Gurfinkel M, Byrne R, Diamond D, Malliaras GG, Benito-Lopez F, Owens RM; Organic Electrochemical Transistor Incorporating an Ionogel as Solid State Electrolyte for Lactate Sensing, *J. Material Chem.* 2012, *22*, 4440-4443

[24] Fabretto M, Zuber K, Hall C, Murphy P, Griesser HJ; The Role of Water in the Synthesis and Performance of Vapour Phase Polymerised PEDOT Electrochromic Devices, *J. Mater. Chem.* **2009**, *19*, 7871-7878

[25] Kukla AL, Shirshov YM, Piletsky SA; Ammonia Sensors Based on Sensitive Polyaniline Films, *Sens. Actuators, B.* **1996**, *37(3)*, 135-140

[26] Yin Y, Feng K, Liu C, Fan S; A Polymer Supercapacitor Capable of Self-Charging under Light Illumination, *J. Phys. Chem.* **2015**, *199(16)*, 8488-8491

[27] Gustafsson G, Cao Y, Treacy M, Klavetter F, Colaneri N, Heeger AJ; Flexible Light-Emitting Diodes Made From Soluble Conducting Polymers, *Nature*. **1992**, *357*, 477-479

[28] Liu Z, Zhou J, Xue H, Shen L, Zang H, Chen W; Polyaniline/TiO$_2$ Solar Cells, *Synth. Met.* **2006**, *156(9-10)*, 721-723

[29] Ke J, Lin G, Hsu C, Chen C, Cheng Y, Jen T, Chen S; Solution Processable Self-Doped Polyaniline as Hole Transport Layer for Inverted Polymer Solar Cells, *J. Mater. Chem.* **2011**, *21(35)***,** 13483-13489

[30] Kaneto K, Kaneko M, Min Y, MacDiarmid AG; "Artificial Muscle": Electrochemical Actuators Using Polyaniline Films, *Synth. Met.* **1995**, *71(1-3)*, 2211-2212

[31] Lam T, Tran H, Yuan W, Yu Z, Ha S, Kaner R, Pei Q; Polyaniline Nanofibers as a Novel Electrode Material for Fault-Tolerant Dielectric Elastomer Actuators, *EAPAD*. **2009**, *6927*

[32] Hemmatian Z, Miyake T, Deng Y, Josberger EE, Keene S, Kautz R, Zhong C, Jin J, Rolandi M; Taking Electrons Out of Bioelectronics: Bioprotonic Memories, Transistors, and Enzyme Logic, *J. Mater. Chem, C*. **2015**, *3*, 6407-6412

[33] Gaylord B, Heeger AJ, Bazan GC; DNA Detection Using Water-Soluble Conjugated Polymers and peptide Nucleic Acid Probes, *Proc. Natl. Acad. Sci*. **2002**, *99*, 10954-10957

[34] Ogura K, Shiigi H, Oho T, Tonosaki T; A CO_2 Sensor with Polymer Composites Operating at Ordinary Temperature, *J. Electrochem. Soc*. **2000**, *147(11)*, 4351-4355

[35] Hossein Hosseini S, Hossein Abdi Oskooei S, Entezami A; "Toxic Gas and Vapour Detection by Polyaniline Gas Sensors", *Iran. Polym. J.* **2005**, *14(4)*, 333-344

[36] Polak AJ, Petty-Weeks S, Beuhler AJ; Applications of Novel Proton-Conducting Polymers to Hydrogen Sensing, *Sens. Actuators*. **1986**, *9(1)*, 1-7

[37] Wang P, Li S, Kan J; A Hydrogen Peroxide Biosensor Based on Polyaniline/FTO, *Sens. Actuators*. **2009**, *137(2)*, 662-668

[38] Irimia-Vladu M, Marjanovic N, Vlad A, Ramil AM, Hernandez-Sosa G, Schooediauer R, Bauer S, Sariciftci NS; Vacuum-Processed Polyaniline-C_{60} Organic Field Effect Transistors, *Adv. Mater.* **2008**, *20(20)*, 3887-3892

[39] Ginder JM, Richter AF, MacDiarmid AG, Epstein AJ; Insulator-to-metal transition in polyaniline, *Solid State Commun.* **1987**, *63(2)*, 97-101

[40] Bernard MC, Hugot-Le Goff A; Quantitative characterization of polyaniline films using Raman spectroscopy I: Polaron lattice and bipolaron, *Electrochim. Acta*. **2006**, *52(2)*, 595-603

[41] Menon R, Yoon CO, Moses D, Heeger AJ, Cao Y; Transport in Polyaniline Near the Critical Regime of the Metal-Insulator Transition, *Phys. Rev. B*. **1993**, *48(24)*, 17685-17694

[42] Genies EM, Lapkowski M; Electrochemical in situ EPR Evidence of Two Polaron-Bipolaron States in Polyaniline, *J. Electroanal. Chem. Interfacial Electrochem.* **1987**, *236(1-2)*, 199-208

[43] Stafstroem S, Bredas JL, Epstein AJ, Woo HS, Tanner DB, Huang WS; Polaron Lattice in Highly Conducting Polyaniline: Theoretical and Optical Studies, *Phys. Rev. Lett*, **1987**, *59(13)*, 1464-1467

[44] Marcus RA; Chemical and Electrochemical electron-transfer Theory, *Annu. Rev. Phys. Chem.* **1964**, *15*, 155-196

[45] Lee K, Cho S, Park SH, Heeger AJ, Lee C, Lee S; Metallic Transport in Polyaniline, *Nature*. **2005**, *441*, 65-68

[46] Gospodinova N, Ivanov DA, Anokhin DV, Mihai I, Vidal L, Brun S, Romanova J, Tadjer A; Unprecidented Route to Ordered Polyaniline: Direct Synthesis of Highly Crystalline Fibrillar Films with Strong π-π Stacking Alignment, *Macromol. Rapid Commun*. **2009**, *30*, 29-33

[47] Kuroda-Wosa T, Munakata M, Matsuda H, Akiyama S, Maekawa M; Syntheses, Structures, and Properties of Copper(I) Co-ordination Polymers with Bridging Phenazine: Construction of One- and Two-Dimensional Structures with Stacking of Phenazine, *J. Chem. Soc. Dalton Trans.* **1995**, *2*, 201-208

[48] Adams PN, Devasagayam P, Pomfret SJ, Abell L, Monkman AP; A New Acid-Processing Route to Polyaniline Films Which Exhibit Metallic Conductivity and Electrical Transport Strongly Dependent Upon Intrachain Molecular Dynamics, *J. Phys.: Condens. Matter*, **1998**, *10(37)*, 8293-8303

[49] Bartlett PN, Birkin PR, Wang JH; An Enzyme Switch Employing Direct Electrochemical Communication Between Horseradish Peroxidase and a Poly(aniline) Film, *Anal. Chem.*, 1998, **70**, pp. 3685-3694

[50] Yang H, Bard A; The application of fast scan cyclic voltammetry. Mechanistic study of the intitial stage of electropolymerization of aniline in aqueous solutions*, *J. Electroanal. Chem.* **1992**, *339*, 423-449

[51] Potje-Kamloth K, Polk BJ, Josowicz M, Janata J; Doping of Polyaniline in the Solid State with Photogenerated Triflic Acid, *Chem. Mater.* **2002**, *14*, 2782-2787

[52] Chao S, Wrighton M; Characterization of a solid-state polyaniline-based transistor: water vapor dependent characteristics of a device employing a poly(vinyl alcohol)/phosphoric acid solid-state electrolyte, *J. Am. Chem. Soc.* **1987**, *109(22)*, 6627-6631

 [53] Wang Y, Liu J, Tran H, Mecklenburg M, Guan X, Stieg AZ, Regan BC, Martin DC, Kaner RB; Morphological and Dimensional Control via Hierarchical Assembly of Doped Oligoaniline Single Crystals, *J. Am. Chem. Soc.* **2012**, *134(22)*, 9251-9262

[54] Jiang KL, Wang JP, Li QQ, Liu LA, Liu CH, Fan SS; Superaligned Carbon Nanotube Arrays, Films, and Yarns: A Road to Applicatoins, *Adv. Mater.* **2011**, *23(9)*, 1154-1161

[55] Jiang KL, Li QQ, Fan SS; Nanotechnology: Spinning Continuous Carbon Nanotube Yarns-Carbon Nanotubes Weave Their Way into a Range of Imaginative Macroscopic Applications, *Nature*. **2002**, *419*, 801

Lebenslauf

Persönliche Daten:

Name:	Aricanli
Vorname:	Kurt
E-Mail:	kurt.aricanli@gmail.com
Geburtsdatum:	10. Juli 1989
Zivilstand:	ledig, keine Kinder

Berufliche Erfahrungen:

04/2012 – 08/2015 Institut für Physikalische Chemie, Linz, Österreich: *Praktikant und Masterarbeiter*

die komplette Herstellung von organische Transistoren mit und ohne Biokonjugation; die Methoden dafür beinhalten Aufdampfen von Metallen (Pd, Au, Cr, Al, LiF), die Anwendung chemischer Einzelschichten (alkylphosphorsäuren und/oder alkylchlorsilan), und die Anwendung organischer Halbleiter kraft einer neuartigen elektrochemischen Herstellung von organischen Halbleiterdünnfilmen (100 nm dick und 60 μm breit) sowie durch das Aufdampfen organischer molekularischen Halbleiterschichten, um elektronische Geräte herzustellen

09/2011 – 11/2011 OSU Abteilung der Molekular Genetik, Columbus OH, USA: *Undergraduate laboratory member*

Betreuung vom Wachstum der Mikroben unter genauer antibiotischen Konzentrationen, Autoklaven für die genetische Umstellung des Arabidopsis Thalianas

03/2010 – 11/2010 University Hospitals Eye Institute, Cleveland OH, USA: *Ohio Amblyope Registry Studie Praktikant*

Analyse von den Diagnostika der Amblyope Patienten (mehr als 1500 Eingaben), Organisation der Messeauftritte im MS Excel

01/2010 – 07/2011	Chemieabteilung OSU allgemeine Chemie, Columbus OH, USA: *Laborfakultät*
	Verwaltung des Labors, Kontrolle der Probestoffe für Experimente, Entsorgung des chemischen Abfalls

Ausbildung:

09/2003 – 06/2007	Euclid High School, Euclid, OH U.S.A.: High school diploma, klassenbester in Mathematik, Bausch&Lomb Honorary Science Award
09/2007 – 12/2011	Die Ohio State Universität, Columbus, OH U.S.A: Abschluss mit dem Bachelor of Science in Biochemie
06/2008 – 08/2008	Bosporus Universität Istanbul, Türkei: Sommerhaftung in einem osmanischen Geschichtekurs.
04/2012 – 02/2016	Johannes Kepler Universität, Linz, Österreich: vorgesehener Abschluss mit Master in WiTech ab Feb. 2016

Sprachen:

Englisch:	Muttersprache
Deutsch:	schriftlich und mündlich sehr gut
Türkisch:	schriftlich und mündlich sehr gut

Spezielle Fähigkeiten:

- geübt in Microsoft Office
- erfahren in Informatik
- Organisationstalent
- unternehmungsfreudig
- flexibel

Freizeit:

Sport, Chemie, Physik, Kochen, Musizieren

Referenzen:

Auf Anfrage

Eidesstattliche Erklärung

Ich erkläre an Eides statt, dass ich die vorliegende Masterarbeit selbständig und ohne fremde Hilfe verfaßt, andere als die angegebenen Quellen und Hilfsmittel benutzt bzw. die wörtlich oder sinngemäß entnommenen Stellen als solche kenntlich gemacht habe.

Die vorliegende Masterarbeit ist mit dem elektronisch übermittelten Textdokument identisch.

Linz, Österreich, März 2016

Kurt Aricanli